Rehabilitation promotes the recovery of distinct functional and structural features of healthy neuronal networks after stoke

Anna Letizia Allegra Mascaro[1,2], Emilia Conti[2†], Stefano Lai[3†], Antonino Paolo Di Giovanna[2], Cristina Spalletti[1], Claudia Alia[4], Eros Quarta[2], Alessandro Panarese[3], Leonardo Sacconi[2,5], Silvestro Micera[3,6], Matteo Caleo[1], Francesco Saverio Pavone[2,5,7]*

1 Neuroscience Institute, National Research Council, Pisa, Italy,
2 European Laboratory for Non-linear Spectroscopy University of Florence, Italy
3 Scuola Superiore Sant'Anna, Pisa, Italy,
4 Scuola Normale Superiore, Pisa, Italy
5 National Institute of Optics, National Research Council, Italy
6 Ecole Polytechnique Federale de Lausanne (EPFL), Lausanne, Switzerland
7 Department of Physics and Astronomy, University of Florence, Italy

Abstract

Rehabilitation is the most effective treatment for promoting the recovery of motor deficits after stroke. Despite its importance, the processes associated with rehabilitative intervention are poorly understood. One of the most challenging experimental goals is to unambiguously link specific circuit changes induced by rehabilitation in recovering animals to improved behavior. Here, we investigate which facets of cortical remodeling are induced by rehabilitative therapy after stroke by combining optical imaging and manipulation tools. We demonstrate the progressive restoration of cortical motor maps and of cortical activity in parallel with the reinforcement of inter-hemispheric connectivity after rehabilitation. Furthermore, we reveal that the increase in vascular density goes along with the stabilization of peri-infarct neural circuitry at synaptic level. The present work provides the first evidences that rehabilitation is sufficient to promote the combined recovery of distinct structural and functional features distinctive of healthy neuronal networks. We believe that understanding the plastic changes induced by rehabilitation will lead to more effective interventions to improve recovery after stroke.

Introduction

Every year, several million stroke victims worldwide are impaired by long-term disability, imparting a large societal and personal burden in terms of lost productivity, lost independence and social withdrawal[1]. Stroke survivors may suffer from lifelong losses in sensory, motor, cognitive, or emotional functioning, depending on the size and localization of the lesion. Persistent motor deficits generally occur after stroke damaged the motor-associated cortices. The recovery of motor function is often only partial, owing to the limited degree of spontaneous brain repair (see for example[2]). On the other hand, strategies that promote brain plasticity, like pharmacological treatments and rehabilitation, can enhance neural rewiring and dramatically improve functional motor outcomes. Pharmacological treatment has been shown to aid the restoration of function in the peri-infarct area. A successful example is the recent study by Carmichael and colleagues demonstrating that administration of a benzodiazepine inverse agonist specific for gamma-aminobutyric acid $GABA_A$ receptors resulted in sustained, improved motor function[3]. Another highly effective rehabilitative approach for restoring motor functions after stroke is physical training[4, 5]. Nevertheless, the lack of complete neuronal repair and functional recovery attained by pharmacological manipulation or motor training alone have led researchers to consider new combination approaches[6]. Thus, neurorehabilitative research is now

seeking to maximize the effectiveness of rehabilitative therapies through a combination of targeted physical exercise and other plasticizing treatments, such as cortical stimulation or pharmacological intervention[7-10], aiming to specifically promote neuronal repair. Many of these treatments act by modulating contralesional hemisphere functionality to counteract disruptive influences of the intact hemisphere on the injured one (see for example[11]), as this interference is often linked with worsened behavioral outcomes in stroke patients[12, 13]. In an effort to unravel the complex mechanism underlying amelioration of motor performances induced by combined therapies, a few animal studies provided useful insights into the associated anatomical adaptations in rodents and primates[8, 14]. Axonal sprouting have been reported following sequential therapy with growth-promoting factors (like Nogo receptor antagonists[14-16] or chondroitinase ABC[17, 18]) and intensive training. In a recent study on mice, Spalletti et al. (under revision) used a rehabilitation paradigm that combines motor training and pharmacological inhibition of the contralesional primary motor cortex (M1) with Botulinum Neurotoxin E (BoNT/E). BoNT/E is known to block neurotransmitter release and synaptic transmission by cleaving SNAP-25, a main component of the SNARE complex[19]. The injection of the toxin transiently counterbalanced the increase in activity in the contralesional hemisphere early after stroke (Spalletti et al., under revision). This theraphy was shown to lead to recovery of motor skills in stroke mice. Importantly, they demonstrated that a combination of the two treatments is necessary to observe a motor improvement that is not task-specific while being generalized to multiple motor functions. The induction of a generalized functional gain, i.e. the recovery of motor functions beyond the ones that are trained, is a crucial aspect to consider in evaluating the efficacy of rehabilitative therapies.

Despite providing essential insights into anatomical and molecular determinants of the behavioral benefits of combined rehabilitation, these studies did not look into the synergistic evolution of the functional maps and their structural counterparts. In that regard, a shortcoming of *ex vivo* studies is that they provide only endpoint measures of reorganization, while dynamic aspects of axonal and dendritic remodeling cannot be evaluated[20]. On the other hand, *in vivo* imaging offers a unique insight into how neurons in the intact nervous system are altered by pathology[20]. In the last decade, wide-field fluorescence or intrinsic signal optical imaging provided valuable insights into spontaneous cortical plasticity after stroke. Murphy and colleagues performed a number of acute studies on cortical remapping after stroke showing with optical imaging techniques the persistence over months of an altered response selectivity of individual neurons and cortical areas[21-23]. In parallel, the high resolution of TPFM has been used to longitudinally evaluate *in vivo* synaptic plasticity after stroke[24]. *In vivo* imaging has shown that the extent of synaptic recovery varies along the distance from the infarct core[25]. Another *in vivo* study found evidence for the redistribution of blood vessel and dendrite orientation confined to the regions near the infarct border a few weeks after photothrombotic stroke[26]. Together with recent investigation of the long-term structural plasticity of dendrites and spines showing a substantial difference in the rewiring of the contralesional vs injured hemisphere after stroke[27-29], these studies provided fundamental insights into the dynamics of spontaneous cortical plasticity after stroke. The availability of a new generation of experimental tools (i.e. optogenetics, transgenesis) for manipulating neuronal activity provide new means of exploring[30, 31] and guiding[32, 33] brain plasticity after ischemia. In combination with the new generation of genetically encoded functional indicators, like GCaMP6[34], optical imaging and optogenetics open new opportunities to dissect longitudinally the neural underpinnings of therapy-aided motor recovery after stroke. In detail, these techniques can fill the gap in our understanding of many fundamental issues related to rehabilitation and brain reshaping to promote recovery.

To our knowledge, no in vivo investigation has yet described on a longitudinal investigation how rehabilitation affects cortical functional and structural plasticity. Many unanswered questions, like how rehabilitation after stroke longitudinally molds cortical functional maps, and how this is associated with modulation of inter-hemispheric connectivity need to be addressed. Furthermore, central issues like the impact of rehabilitation on neuronal structural plasticity are inadequately investigated. Finally, how neurons and vasculature, crucial determinants of cortical rewiring, act in concert to determine this complex and manifold plastic reshaping is still to be defined.

In the present study, we dissected how rehabilitative treatment activates concurrent modalities of cortical plasticity in mice by using a multimodal approach that combines cutting-edge optical imaging and manipulation techniques. By a longitudinal evaluation of cortical functional remodeling, we found that a combination of physical training with pharmacological manipulation of the contralesional activity is necessary to restore essential features of pre-stroke conditions of the activation profiles, both in spatial and temporal terms. In the same animals presenting large-scale remapping of the injured hemisphere, we found a significant enhancement of transcallosal functional connectivity after one month of rehabilitative therapy. Furthermore, our experiments reveal an increase in the density of blood vessels primarily focused in the peri-infarct area, suggesting that the functional reshaping is supported by the neurovascular syncytium. Finally, as structural backbone of this modified functionality, we found in the same double-treated subjects that preservation of dendritic architecture goes along with stabilization of spines in the peri-infarct region. Overall, our study provides unprecedented view of complimentary aspects of cortical anatomical and functional adaptation induced by rehabilitation after stroke.

Results

Experimental design

We used a photothrombotic model of focal stroke applied to the right M1 of GCaMP6f or GFPM mice (STROKE, ROBOT and REHAB groups). The combined rehabilitation paradigm of the REHAB group consists in a combination of highly repeatable motor training of the mouse forelimb in a robotic platform (M-Platform[35]) and reversible pharmacological inactivation of the healthy, contralesional hemisphere via the synaptic blocker Botulinum Neurotoxin E (BoNT/E; see Supplementary Fig. 1A). The ROBOT group performed the same daily training on the M-platform as REHAB mice, but without pharmacological treatment. Rehabilitation-associated training on the M-Platform consisted of repeated cycles of passively actuated contralesional forelimb extension followed by its active retraction triggered by an acoustic cue (Fig. 1A and Supplementary Fig. 1B).

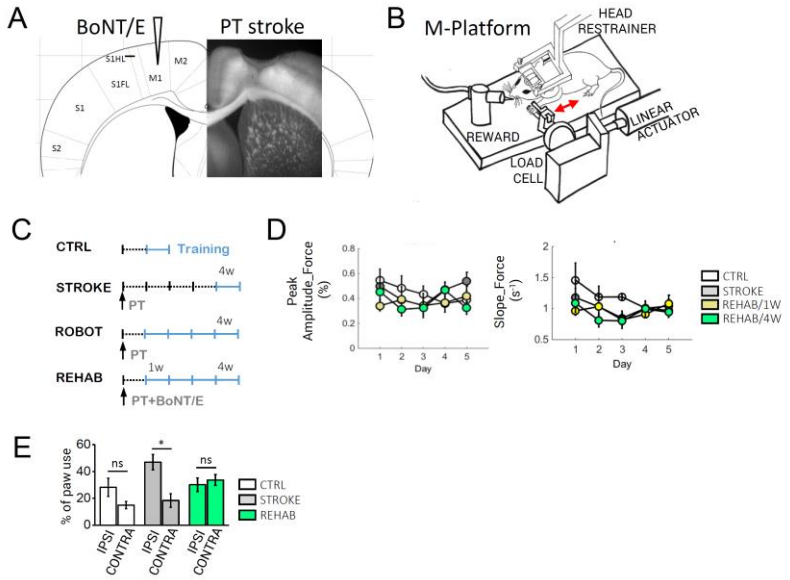

Supplementary Figure 1. **Experimental design.** (A) A schematic of the experimental protocol, which combines the photothrombotic stroke in the primary motor cortex (M1) with a contralesional injection of BoNT/E into the homotopic cortex. (B) A schematic representation of the M-Platform that was used for rehabilitative training. (C) The experimental timeline for the CTRL, STROKE and REHAB groups in the awake imaging experiment. Light blue lines refer to training weeks. W = week; PT = photothrombosis. (D) Graphs showing the Peak amplitude (left) and Slope (right) of the force signals recorded in the pulling phase during training on the M-Platform over 5 days (4 weeks after injury for STROKE mice, 1 and 4 weeks after injury for REHAB mice, during the week of training for CTRL mice). There is no significant difference between the groups and over the 5 days. (E) Histogram showing the % of ipsilateral versus contralateral paw use in the Schallert cylinder test performed 30 days post stroke by GCaMP6f mice ($Nmice_{CTRL}$= 3, $Nmice_{STROKE}$ = 3, $Nmice_{REHAB}$= 3, $CTRL_{IPSI}$=28 ± 7%; $CTRL_{CONTRA}$=15 ± 3%; $STROKE_{IPSI}$=47 ± 6%; $STROKE_{CONTRA}$=18 ± 5%; $REHAB_{IPSI}$ = 30 ± 5%; $REHAB_{CONTRA}$ = 34 ± 4%; t-test $STROKE_{IPSI}/STROKE_{CONTRA}$ * P = 0.01). IPSI and CONTRA refer to the ipsilesional and contralesional paws, respectively; ns, not significant.

ROBOT and REHAB mice were trained for 4 weeks starting 5 days after injury (Supplementary Fig. 1C), in line with the overall consensus that the initiation of rehabilitative training 5 or more days after stroke is mostly beneficial and has no adverse effects[36]. The motor task was rapidly learned and easily performed. Indeed, the performances, evaluated by the amplitude and slope of the force peaks exerted during the voluntary forelimb-pulling task, were not significantly different across groups, within a week nor across weeks of training (Supplementary Fig. 1D). The treatment induced a generalized improvement in motor performance, as assessed by the Schallert Cylinder test[37] one month after the lesion. While the STROKE mice showed a significant asymmetry in forelimb use, this impairment was no longer present in REHAB mice at 30 days post-stroke (Supplementary Fig. 1E).

Combined rehabilitation treatment restores cortical activity patterns disrupted by stroke

To assess the extent to which the improved motor performance was accompanied by large- and small-scale plastic rearrangements of cortical networks, we investigated the remapping of motor representations, vascular network remodeling and synaptic dynamics. First, we evaluated how rehabilitation modulated cortical functionality in these mice. To do this, we implemented an integrated system for simultaneous calcium imaging over the meso-scale using the calcium indicator protein GCaMP6f, and the recording of forces applied by the contralesional forelimb during the training sessions on the M-Platform (Fig. 1A-C). Calcium imaging was used as a measure of the cortical activity in the brains of GCaMP6f mice. Wide-field calcium imaging showed that a small area located in the motor-sensory region reproducibly lighted up in CTRL mice during the M-platform forelimb retraction movement (an example of cortical activation is reported in Fig. 1D and Supplementary Fig. 2A). On the contrary, a large area covering most of the cortical surface of the injured hemisphere was activated synchronously in non-treated (STROKE) mice one month after stroke while performing the task. We initially tested if 4 weeks of motor training on the M-platform (ROBOT group) could restore pre-stroke conditions. We observed that motor rehabilitation without pharmacological intervention resulted in a diffuse activation, originating from the peri-infarct cortex (Supplementary Fig. 2A). Remarkably, in comparison to STROKE and ROBOT mice, REHAB mice showed a more spatially restricted zone of

activation that was similar to the pattern seen in healthy controls (CTRL) in terms of location, timing and amplitude (Fig. 1D-H, Supplementary Fig. 2A-D). By overlapping the forelimb retraction-triggered cortical maps obtained on every day of the training week, we quantified the location and origin of activation of the calcium waves (Supplementary Fig. 2B-D). Stroke shifted and expanded the location of the retraction task motor representation from M1 toward more caudal brain regions not specifically associated with motor control in STROKE mice (Supplementary Fig. 2C, 2nd panel). ROBOT mice showed a cortical activation that positively correlated with proximity to the stroke lesion, but more diffuse compared to CTRL mice (Supplementary Fig. 2C, 3rd and 1st panel, respectively, and Supplementary Fig. 2D). Interestingly, the spread of cortical activation in REHAB mice was further reduced towards pre-stroke conditions (Supplementary Fig. 2C 4th panel and Supplementary Fig. 2D). In most cases (5 out of 6 REHAB mice), the improvement in cortical activation patterns was associated with increased functional connectivity between the primary and secondary motor output areas at the end of the training period (REHAB/4W) compared to the beginning (REHAB/1W), towards healthy (CTRL) conditions (Supplementary Fig. 2E).

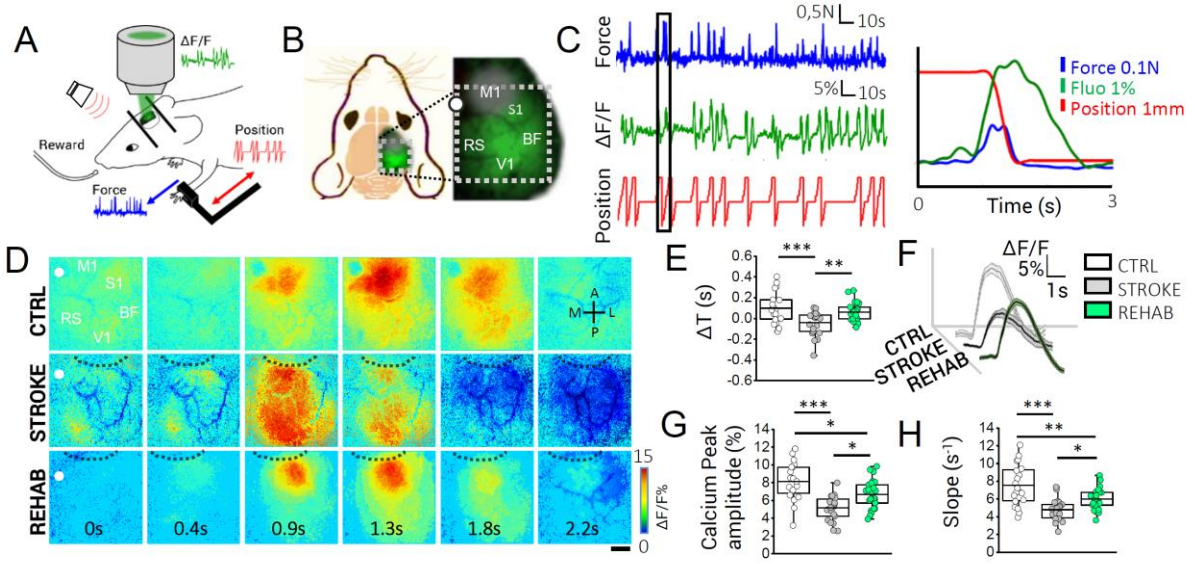

Figure 1: **Combined rehabilitation counteracts cortical dedifferentiation and restores cortical activation profiles in the post stroke, peri-infarct region**. (A) A schematic representation of the M-Platform used for rehabilitative training and simultaneous calcium imaging, which was used as a measure of cortical activity. Examples of force (blue), position (red) and ΔF/F traces (green) are reported. (B) A schematic representation of the field of view (i.e. the area within the dotted white square) used for wide-field calcium imaging in GCaMP6f mice. The gray circular "cloud" on the M1 region highlights the location and approximate extent of the lesion. M1, primary motor area; S1, primary somatosensory area; BF, barrel field; V1, primary visual cortex; RS, retrosplenial cortex. The white dot indicates the bregma. (C) An example of the force trace recorded by the load cell during the passive-extension, active-retraction trials on the rehabilitative platform (blue trace), the simultaneously recorded calcium fluorescence trace (green trace) and the position of the handle (red trace). The graph on the right shows an overlap of the simultaneously recorded traces that correspond to the black box on the left. (D) An image sequence of cortical activation as assessed by calcium imaging during pulling of the handle by the contralateral forelimb, from 0.4 s before to 1.8 s after the onset of the force peak. Each row shows a representative sequence from a single animal of each group. Black dashed lines define the lesion borders; the white dot indicates bregma. Scale bar, 1mm. (E) The delays in cortical activation in caudal regions in response to contralateral forelimb retraction are shown for the 3 groups ($Nmice_{CTRL}$= 4, $Nmice_{STROKE}$ = 6, $Nmice_{REHAB}$= 6; ΔT_{CTRL} = 0.10 ± 0.03 s, ΔT_{STROKE} = -0.04 ± 0.02 s, ΔT_{REHAB}= 0.06 ± 0.02 s; one-way analysis of variance (ANOVA) followed by the Bonferroni test: *** P = 0.0007, ** P = 0.01). (F) Average calcium traces recorded in the region of maximal activation, ROI_8 (see Methods), during contralateral forelimb retraction for the three experimental groups; the shadows indicate the SEM values. (G) The graph shows the maximum of the fluorescence peaks from the same calcium traces as in (F) (Peak $amplitude_{CTRL}$ = 8.1 ± 0.5 %; Peak $amplitude_{STROKE}$ = 5.2 ± 0.3%; Peak $amplitude_{REHAB}$ = 6.6 ± 0.3%; one-way ANOVA followed by the Bonferroni test: *** P =$9*10^{-7}$, * *P (CTRL/REHAB)* = 0.03, * *P (STROKE/REHAB)* =0.02). (H) The graph shows the slope (average ± SEM) of the fluorescence in the rising phase of the trace ($Slope_{CTRL}$ = 7.5 ± 0.5 s^{-1}; $Slope_{STROKE}$ = 4.8 ± 0.2 s^{-1}, $Slope_{REHAB}$ = 6.0 ± 0.2 s^{-1}; one-way ANOVA followed by the Bonferroni test: *** P =$6*10^{-7}$, ** P = 0.007, * P = 0.05).

Our results indicate that the combined rehabilitative treatment focalizes the cortical activation to the peri-infarct region while limiting the concurrent recruitment of distant locations.

We hypothesized that the spatial spread of calcium waves implied a synchronicity in the activation of the rostral peri-infarct network and the caudal inter-connected region. By analyzing the temporal profile of forelimb retraction-triggered cortical activation, we found that the delay between the maximum calcium peak of the rostral and caudal regions was reversed in STROKE versus CTRL mice, indicating that the activation of the caudal region somewhat preceded the activation of the peri-infarct areas in STROKE mice (Fig. 1E). Longitudinal imaging showed a progressive recovery of the average calcium activation temporal dynamics in REHAB mice during the 4 weeks of training (Supplementary Fig. 2F, left panel). The spatio-temporal profile of the REHAB group closely resembled CTRL animals, suggesting that the motor output pattern underlying the forelimb retraction primarily involved the peri-infarct region. Furthermore, we found that the combined treatment profoundly affected the neuronal activation patterns of REHAB mice. Indeed, the average calcium imaging fluorescence traces in Fig. 1F show the differences in the calcium dynamics measured in the region of maximum activation (*ROIg*, see Supplementary Fig. 2B) during contralateral forelimb retraction in CTRL, STROKE, and REHAB mice.

While a significant reduction in the amplitude of the cortical activity during forelimb retraction was evident one month after stroke in the STROKE group, the amplitude in cortical activation in in REHAB mice partially recovered to pre-stroke conditions (Fig. 1G). The combined treatment led to the progressive increase in the amplitude of the calcium response (Supplementary Fig. 2F, middle panel). Moreover, REHAB animals showed progressively steeper slope of calcium activation during the rehabilitation period (Supplementary Fig. 2F, right panel), implying more rapid cortical activation. As compared to STROKE animals, REHAB mice demonstrated a faster calcium activation curve during the forelimb retraction task after 4 weeks of training (Fig. 1H).

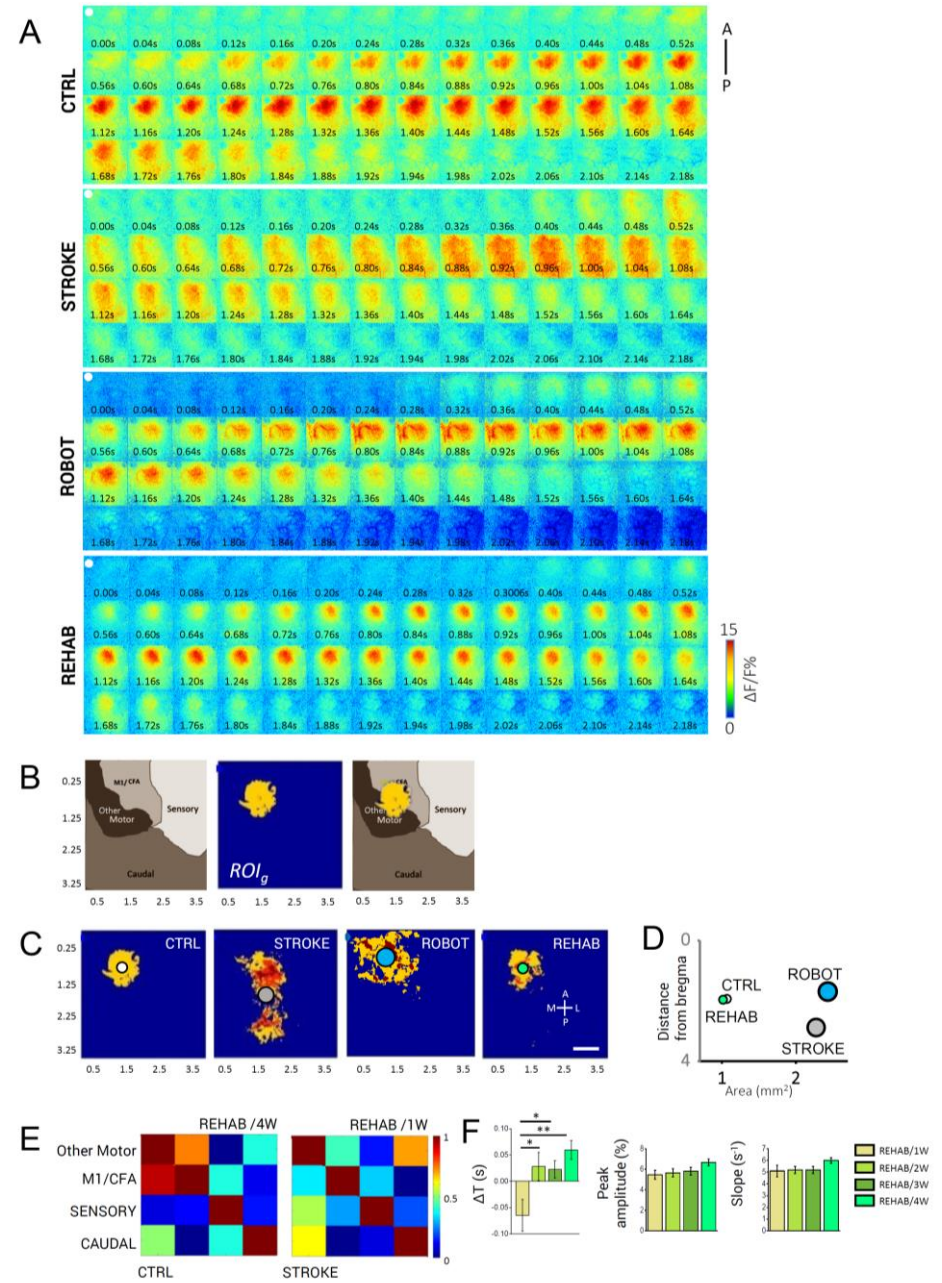

Supplementary Figure 2: **Wide-field imaging of cortical activation profiles over 4 weeks of rehabilitation**. (A) Complete image sequences of cortical activation as assessed by calcium imaging during pulling of the handle by the contralateral forelimb of CTRL (top), STROKE (middle) and REHAB (bottom) GCaMP6f mice in the M-Platform. A-P, anterior-posterior. The white dot indicates bregma. Scale bar = 1 mm. (B) The image of the left shows a functional map based on the intracortical microstimulation (ICMS) studies of Tennant (2011, Cerebral Cortex) and Alia (2016, Sci Reports) that was used as a reference map. The middle panel shows the average thresholded ROI (*ROI$_g$*) computed for CTRL animals during voluntary contralateral forelimb pulling in the M-Platform. The image on the right shows a merged image of the functional map and *ROIg*. CFA, caudal forelimb area. The caudal area includes visual and associative regions. (C) The panels show the average thresholded ROI (*ROI$_g$*) computed for each experimental group. The circles represent the centroids of the *ROI$_g$* for CTRL (white), STROKE (light gray), ROBOT (blue) and REHAB (green) groups. Scale bar = 1 mm. (D) The areas of the *ROI$_g$* and their distance from bregma are presented in the scatter plot. (E) Examples of partial correlation matrices of cortical activation during voluntary pulling. The correlation analysis on REHAB mice was performed based on two evaluation time points: one week (REHAB/1W) and four weeks (REHAB/4W) after stroke. (F) Longitudinal analysis of cortical activation profiles over the four rehabilitation weeks. Graphs in the left, middle and right panels are calculated as in Fig. 1E, G, and H, respectively. Left panel: Delays in cortical activation in caudal regions following the forelimb retraction task are reported for the 4 weeks of rehabilitative training ($Nmice_{REHAB}$= 6; $\Delta T_{REHAB/1W}$ = -0.06 ± 0.03 s, $\Delta T_{REHAB/2W}$ = -0.03 ± 0.03 s, $\Delta T_{REHAB/3W}$ = 0.02 ± 0.02 s, $\Delta T_{REHAB/4W}$ = 0.06 ± 0.02 s; one-way ANOVA followed by the Tukey test: ** P <0.01, *P <0.05; REHAB/4W here corresponds to the REHAB group in all the other panels). Middle panel: the maximum of calcium imaging fluorescence peaks for the 4 weeks of rehabilitative training ($Nmice_{REHAB}$= 6; Peak $amplitude_{REHAB/1W}$= 5.4 ± 0.4%, Peak $amplitude_{REHAB/2W}$ = 5.6 ±0.4 %, Peak $amplitude_{REHAB/3W}$ = 5.8 ± 0.4%, Peak $amplitude_{REHAB/4W}$ = 6.6 ± 0.3 %; No significant changes were observed over the 4 weeks period). Right panel: The graph shows the slope (average ± SEM) of the calcium imaging fluorescence in the rising phase ($Nmice_{REHAB}$= 6; $Slope_{REHAB/1W}$= 5.1 ±0.5 s^{-1}, $Slope_{REHAB/2W}$= 5.2 ±0.3 s^{-1}, $Slope_{REHAB/3W}$= 5.2 ±0.3 s^{-1}, $Slope_{REHAB/4W}$= 6.0 ±0.2 s^{-1}; No significant changes were observed over the 4 weeks period).

We observed that the training on the M-Platform for 4 weeks alone (ROBOT mice) resulted in a small but not significant improvement in calcium kinetics parameters compared to STROKE mice (Supplementary Fig. 3).

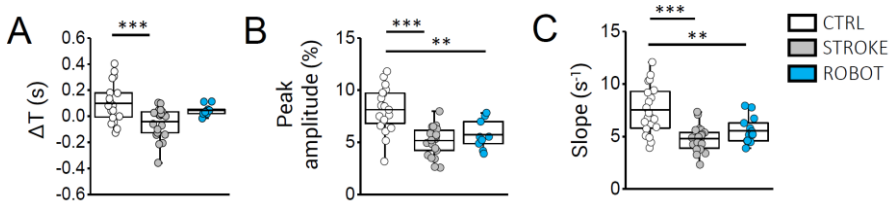

Supplementary Figure 3: **Motor training on the M-platform is not sufficient to trigger recovery of cortical activity patterns.** (A) The delays in cortical activation in caudal regions in response to contralateral forelimb retraction are shown for the 3 groups ($Nmice_{CTRL}$= 4, $Nmice_{STROKE}$ = 6, $Nmice_{ROBOT}$= 3; ΔT_{CTRL} = 0.10 ± 0.03 s, ΔT_{STROKE} = -0.04 ± 0.02 s, ΔT_{ROBOT}= 0.05 ± 0.01 s; one-way analysis of variance (ANOVA) followed by the Bonferroni test: *** P = 0.0007). (B) The graph shows the maximum of the fluorescence peaks from the same calcium traces as in (A) (Peak $amplitude_{CTRL}$ = 8.1 ± 0.5 %; Peak $amplitude_{STROKE}$ = 5.2 ± 0.3%; Peak $amplitude_{ROBOT}$ = 5.7 ± 0.5%; one-way ANOVA followed by the Bonferroni test: *** $P = 9*10^{-7}$, ** P = 0.004). (C) The graph shows the slope of the fluorescence in the rising phase of the trace ($Slope_{CTRL}$ = 7.5 ± 0.5 s-1; $Slope_{STROKE}$ = 4.8 ± 0.2 s-1, $Slope_{ROBOT}$ = 5.5 ± 0.3 s-1; one-way ANOVA followed by the Bonferroni test: *** $P = 6*10^{-7}$, ** P = 0.02). All values are reported as average ± SEM.

On the contrary, the combined treatment (REHAB mice) promoted a more solid rescue of calcium kinetics significantly different from STROKE mice towards heathy conditions (Fig. 1E-H). Based on the modest changes induced by motor training in the ROBOT group on cortical functionality, we decided to focus the analysis of others plasticity modules investigated in the following experiments exclusively on the combined treatment (REHAB group).

In brief, our results show that the combined rehabilitative treatment is necessary to promote the recovery of the temporal and spatial features of the cortical activation patterns in the peri-infarct region that are associated with the execution of a motor task.

Comprehensive optical investigation reveals a rehabilitation-induced enhancement of inter-hemispheric functional connectivity

Having analyzed the ipsilateral adaptation of cortical activity, we next evaluated how distal interconnected regions, such as the contralesional motor cortex, were affected by our therapeutic intervention. Several studies in mice and humans have shown that interhemispheric M1 connectivity is reduced after stroke[38-40]. Increased interhemispheric connectivity is hypothesized to positively correlate with the recovery of motor performance in the subacute stage after stroke in humans[41]. Based on this hypothesis, we tested whether transcallosal connectivity between homotopic areas was modulated by the double rehabilitative treatment by using an all-optical approach that combines optogenetic activation of the intact M1 with calcium imaging of the cortex in the injured hemisphere. In these experiments, the spared, left M1s of GCaMP6f mice were injected with AAV9-CaMKII-ChR2-mCherry to induce the expression of ChR2 in excitatory neurons (Fig. 2A).

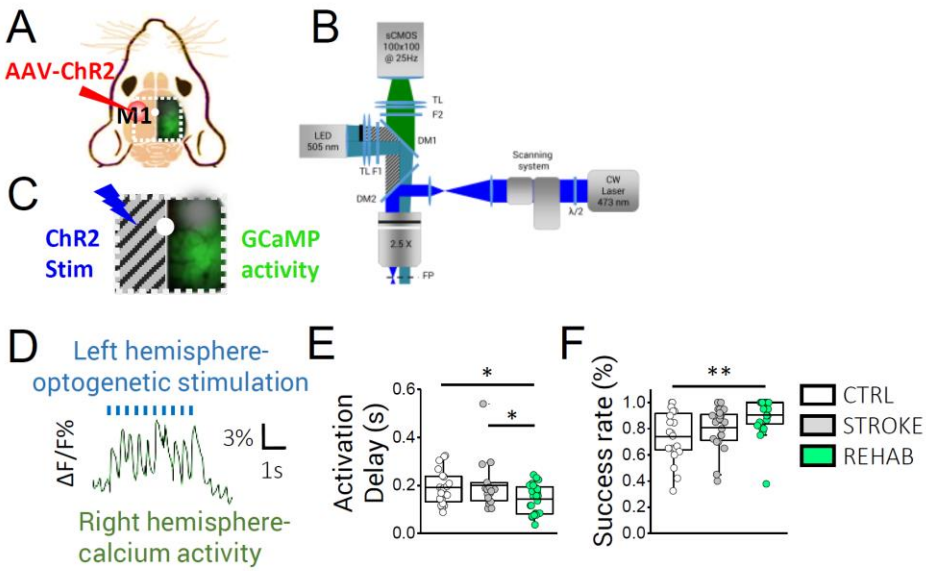

Figure 2: **Combined rehabilitation induces strengthened interhemispheric connectivity after stroke.** (A) A schematic representation of the field of view (i.e. the area within the white dotted square) for the all-optical investigation of inter-hemispheric functional connectivity in GCaMP6f mice. The red circle in the left hemisphere indicates M1 injected with AAV-ChR2-mCherry; the gray circular "cloud" labels the site of the stroke lesion in the right hemisphere. The white dot indicates bregma. (B) A schematic representation of the wide-field microscope with a double illumination path that allows simultaneous light stimulation for optogenetics and fluorescent recording for calcium imaging. The hemi-occlusion of the 505nm LED, displayed by the black line on the upper half of the LED illumination path, avoids spurious ChR2 stimulation during calcium imaging. TL, tube lens; F1/2, band-pass filters; DM1/2, dichroic mirror; FP, focal plane. (C) The panel shows the simultaneous ChR2 laser stimulation on the left hemisphere (not illuminated by LED light) and the detection of the evoked GCaMP6f fluorescence on the right side. (D) A trace of optogenetically elicited calcium activity in the right cortex. (E) Box and whiskers plot showing the delay between the onset of left hemisphere laser stimulation and the peak of the calcium responses in the right hemisphere (average ± SEM; $Nmice_{CTRL}$ = 4, $Nmice_{STROKE}$ = 3, $Nmice_{REHAB}$ = 3; Activation $Delay_{CTRL}$ = 0.19 ± 0.02 s, Activation $Delay_{STROKE}$ = 0.20 ± 0.02 s, Activation $Delay_{REHAB}$ = 0.14 ± 0.01 s; one way ANOVA post hoc Fisher, P <0.05 for all comparisons;). (F) The success rate (SR) of laser stimulation, calculated as the number of times the laser stimulation successfully triggered contralateral activation over the total number of stimulation trials (average ± SEM, same Nmice as in (E); SR_{CTRL}= 0.74 ± 0.04, SR_{STROKE}= 0.81 ± 0.03, SR_{REAHAB}= 0.90± 0.03; ANOVA with post hoc Bonferroni test: P < 0.01).

One month after stroke, we optogenetically stimulated the spared M1. To avoid ChR2 stimulation while exciting GCaMP6f fluorescence, we partially occluded the 505 nm LED in our custom-made wide-field microscope (Fig. 2B-C). Optogenetic stimulation was achieved by taking advantage of a second excitation path in which a 470 nm laser was focused on the AAV-transfected region via acousto-optic deflectors (AODs). Laser stimulation of the contralesional M1 reproducibly triggered calcium waves in the injured hemisphere (Fig. 2D, Supplementary Video 1), beginning mainly in the homotopic M1 of CTRL mice, but in the peri-infarct area of STROKE and REHAB animals (Supplementary Fig. 4).

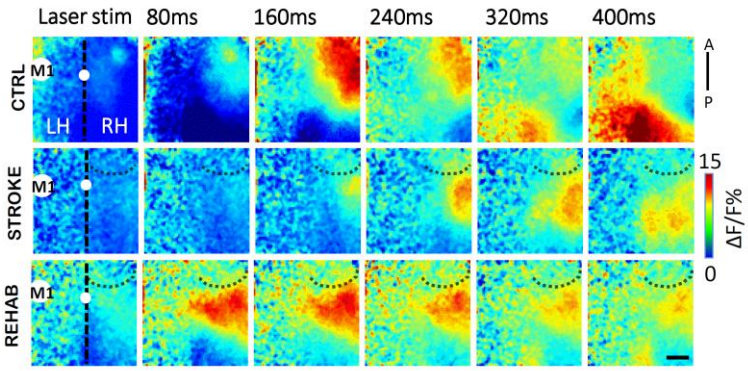

Supplementary Figure 4: **Optogenetically triggered activation of contralateral hemisphere.** Representative image sequences from a single animal in each group showing ipsilesional cortical activation as assessed by calcium imaging following 473 nm laser stimulation (1 Hz, 5ms pulse duration) of the ChR2-expressing intact M1. The white spot on the vertical black dotted line (midline) indicates bregma. The dotted curve lines highlight the area injured by stroke. A,P: anterior, posterior. LH, left hemisphere; RH, right hemisphere. Scale bar = 1 mm.

Afterwards, calcium waves propagated to functionally connected regions that were located either anterior or posterior to the primary source of activation in all 3 groups of animals (Supplementary Video 1).By visual inspection, the temporal dynamics of the calcium waves were comparable between CTRL

and STROKE mice (Supplementary Fig. 4). Indeed, we quantified the delay between the start of the optogenetic stimulation of the left hemisphere and the peak of calcium activity in the right hemisphere, and found no significant difference between the STROKE and CTRL mice (Fig. 2E). In contrast, the delay between the delivery of the optogenetic stimulus and the calcium response in the right hemisphere was significantly reduced in REHAB mice as compared to both CTRL and STROKE mice (Fig. 2E). In parallel, the success rate of contralateral activity in response to optogenetic stimulation was higher in REHAB mice than in CTRL and STROKE animals (Fig. 2F). Therefore, this series of all-optical experiments suggests that combined rehabilitation after stroke strengthens the functional connectivity between the spared motor cortex and the perilesional cortex.

Combined rehabilitative treatment stimulates angiogenesis in the peri-infarct area

We next assessed whether vascular reorganization represented a structural correlate of the functional remapping that occurred at the local and inter-hemispheric levels in REHAB animals after stroke. To test this, we observed longitudinally imaged mouse cortices of all groups under both the cranial window and the thinned skull preparations in the month following the induced stroke, and found that the injured area consistently shrunk owing to the collapse of dead tissue in STROKE and REHAB mice (Fig. 3A and 4A). In addition, a very bright area appeared in the peri-infarct region of both groups of GCaMP6 mice, possibly representing an excitotoxic response associated calcium dysregulation[42] elicited by the photothrombotic stroke (see the left panel of Fig. 3A; 13 out of 14 STROKE and REHAB mice). The enhanced brightness gradually diminished and disappeared after the acute period (6-19 days after injury in STROKE and REHAB mice; see example in Fig. 3A, right panel), and was accompanied by a large shrinkage of the necrotic tissue. The consequent displacement of the peri-infarct area was associated with a substantial remodeling of blood vessels (white arrowheads in Fig 3A), in agreement with previous studies[26].

To quantify the structural vascular reshaping associated with stroke and rehabilitation, we performed 3D reconstructions of the cortical vasculature. Specifically, after the last motor training session, we stained the brain vasculature of GFPM mice with a vessel-filling fluorescent dye, albumin-fluorescein isothiocyanate (FITC, Fig. 3B). By performing TPFM on Thiodiethanol (TDE) cleared cortical slices (see Methods), we obtained high-resolution 3D maps of blood vessels of the injured, right hemisphere (Fig. 3C, Supplementary Video 2). A strong orientation gradient of blood vessels induced by the collapse of dead tissue in the ischemic core was evident in both the STROKE and REHAB groups. Indeed, combined rehabilitative treatment did not rescue random vascular orientation of pre-stroke conditions in regions proximal (<500 µm) or distal (1000 to 1500 µm from core) to the stroke core in REHAB mice (Fig. 3D-E).

On the other hand, the density of blood vessels near the infarct site was significantly higher in REHAB mice than in CTRL and STROKE groups (Fig. 3F, left panel). We further evaluated the vascular density over the entire cortical depth to define each layer-specific contribution to the overall increase in blood vessel density in REHAB animals. The blood vessel distribution was uniform in both CTRL and STROKE mice. Increases in density localized mainly to the middle and deeper layers of the cortex (300-700 µm deep) in the REHAB group (Fig. 3F, middle panel). We found that this layer-specific increased vascular density in the REHAB animals, which was possibly due to treatment-induced angiogenesis, is mainly observed in the region proximal to the stroke core (Fig. 3F, right panel).

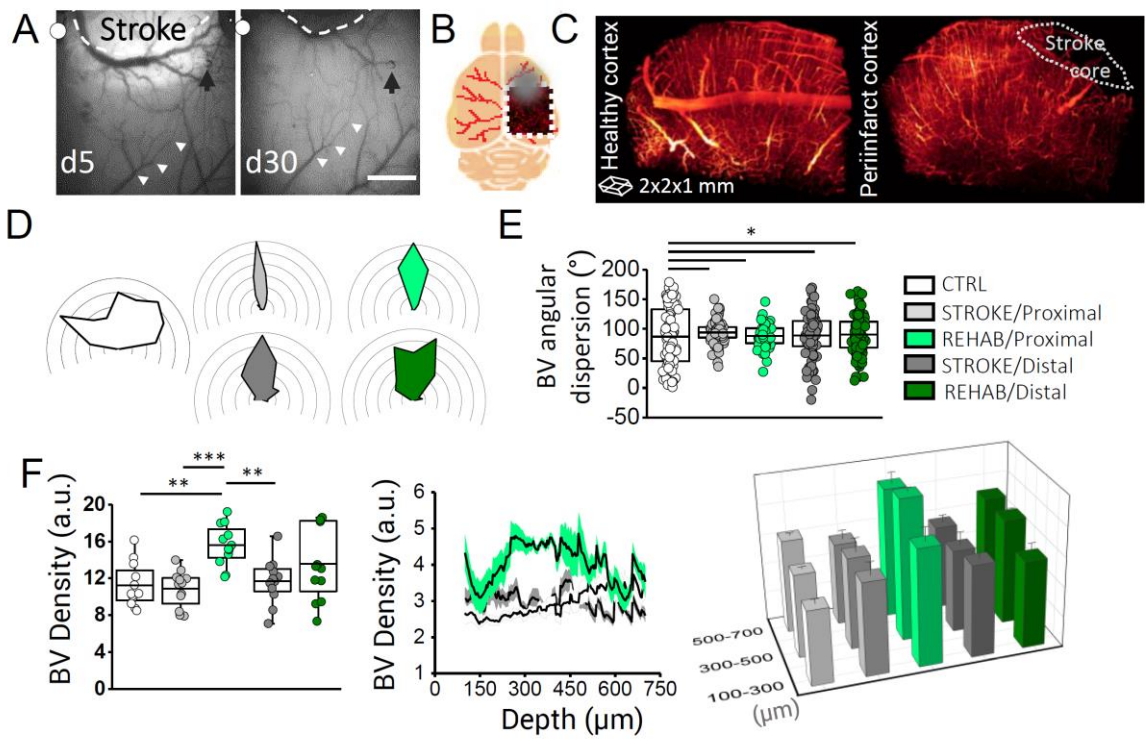

Figure 3: **Combined rehabilitation promotes angiogenesis in the peri-infarct area**. (A) Brightfield images showing the cortical vasculature following a stroke under a thinned skull preparation. The dotted line emphasizes the profile of a large blood vessel shifting toward the stroke core from 5 days to 30 days after stroke; a similar shift is highlighted by the white arrowheads on a blood vessel distal to the injury site. The black arrow points to an internal reference on the image. The white dots indicate bregma. (B) A schematic representation of the fixed brain of a GFPM mouse, in which the vasculature is labeled with TRITC (red lines). The dotted square highlights the imaged area; the circular gray "cloud" labels the stroke location. (C) A 3D meso-scale reconstruction of the vasculature in the healthy contralesional cortex (left) and in the peri-infarct area (right) from TDE-cleared cortical slices obtained from a STROKE GFPM mouse, one month after injury. The white dotted region highlights the absence of blood vessels in the infarct core. (D) The polar plot shows the distribution of blood vessel orientation in regions proximal and distal to the core for each experimental group measured after the last motor training session ($Nmice_{CTRL}$ = 3; $Nmice_{STROKE}$ = 3; $Nmice_{REHAB}$ = 3). The plots are oriented as in Fig. 3A; the lesioned area is toward the uppermost centre of the plot. (E) Box and whiskers plot of the angular distribution of the vasculature in proximal (<500 µm) or distal (1000 to 1500 µm) regions from the stroke core of each experimental group measured after the last motor training session (Blood vessel angular dispersion: $BVAD_{CTRL}$ = 87 ± 5°; $BVAD_{STROKE\ Proximal}$ = 94 ± 2°; $BVAD_{STROKE\ Distal}$ = 89 ± 4°; $BVAD_{REHAB\ Proximal}$ = 88 ± 2°; $BVAD_{REHAB\ Distal}$ = 90 ± 4°; Homogeneity of variance test: F=34.3; all variances significantly different from CTRL). (F) Blood vessel (BV) density analysis. *(Left)* The histogram shows the blood vessel density (average ± SEM) in proximal and distal regions from the stroke core in each experimental group ($BV\ Density_{CTRL}$ = 11.2 ± 0.7 a.u.; $BV\ Density_{STROKE\ Proximal}$ = 10.9 ± 0.6; $BV\ Density_{STROKE\ Distal}$ = 11.7 ± 0.6; $BV\ Density_{REHAB\ Proximal}$ = 15.6 ± 0.7; $BV\ Density_{REHAB\ Distal}$ = 13.6 ± 1.1; one-way ANOVA with post hoc Bonferroni test: *** P <0.001, ** P <0.01, * P <0.01). *(Middle)* The traces indicate the blood vessel density with respect to brain cortex depth in each experimental group. Gray shadows represent the SEM. *(Right)* A 3D graph comparing the average blood vessel density grouped by cortical depth (100-300 µm from stroke core: $BV\ Density_{CTRL}$ = 2.5 ± 0.2; $BV\ Density_{STROKE\ Proximal}$ = 3.1 ± 0.4; $BV\ Density_{REHAB\ Proximal}$ = 3.9 ± 0.5; $BV\ Density_{STROKE\ Distal}$ = 3.1 ± 0.4; $BV\ Density_{REHAB\ Distal}$ = 2.9 ± 0.4; 300-500 µm from stroke core: $BV\ Density_{CTRL}$ = 2.8 ± 0.1; $BV\ Density_{STROKE\ Proximal}$ = 3.1 ± 0.5; $BV\ Density_{REHAB\ Proximal}$ = 4.7 ± 0.2; $BV\ Density_{STROKE\ Distal}$ = 2.8 ± 0.5; $BV\ Density_{REHAB\ Distal}$ = 3.5 ± 0.2; 500-700 µm from stroke core: $BV\ Density_{CTRL}$ = 3.1 ± 0.1; $BV\ Density_{STROKE\ Proximal}$ = 2.8 ± 0.3; $BV\ Density_{REHAB\ Proximal}$ = 4.4 ± 0.4; $BV\ Density_{STROKE\ Distal}$ = 2.8 ± 0.3; $BV\ Density_{REHAB\ Distal}$ = 3.6 ± 0.1; 300-500 µm from the stroke core: P <0.05 for REHAB Proximal vs STROKE Proximal, STROKE Distal, and CTRL; 500-700 µm from the stroke core: P <0.05 for REHAB Proximal vs STROKE Proximal and STROKE Distal, one-way ANOVA with post hoc Bonferroni test).

In conclusion, by combining *in vivo* and *ex vivo* imaging methods, we generated 3D cortical vascular maps and observed a pro-angiogenic effect of the combined rehabilitative treatment on the vasculature of the peri-infarct area.

Combined rehabilitation preserves pyramidal neurons architecture and promotes the stabilization of synaptic contacts in the peri-infarct area

In parallel with vascular reshaping, we explored potential finer neuro-anatomical adaptations to define their contribution to changes in cortical activity after stroke. Heightened spontaneous structural

remodeling has been observed in animals in both presynaptic (axonal fibers and terminals) and postsynaptic (dendrites and dendritic spines) neuronal structures in the peri-infarct cortex in the weeks following stroke[43-47]. In the next set of *in vivo* experiments, we aimed at defining if rehabilitation after stroke is associated with an alteration in synaptic-level cortical circuits, and how this change is modulated by distance from the core. We performed TPFM of pyramidal apical dendrites and axons (up to 100 µm deep relative to the pial surface) at increasing distances (up to 4 mm) from the stroke core in the cortex of GFPM mice. The imaging area overlapped with the region visualized in GCaMP6f mice (Supplementary Fig. 5A). The orientation of dendrites and axons was evaluated on the 4th week after injury in STROKE and REHAB mice. In the same animals studied on the vascular imaging experiments, we show that the reorganization of cortical tissue (Fig. 4A, left panels) that led to a considerable alignment of blood vessels towards the stroke core produced an analogous re-orientation of cortical dendrites and axons in the peri-infarct area of STROKE mice (white arrow in Fig. 4A, right panels). Reorientation was less pronounced in these animals at distal regions from the ischemic core (>1 mm; Supplementary Fig. 5C). In contrast, the change in organization of pyramidal processes was not visible in REHAB animals (Fig. 4B and Supplementary Fig. 5B) even though stroke profoundly altered the spatial distribution of blood vessels around the stroke core in the same mice. Indeed, the randomness in dendrite orientation typical of healthy subjects was preserved in REHAB mice as compared to the STROKE group (Fig. 4B).

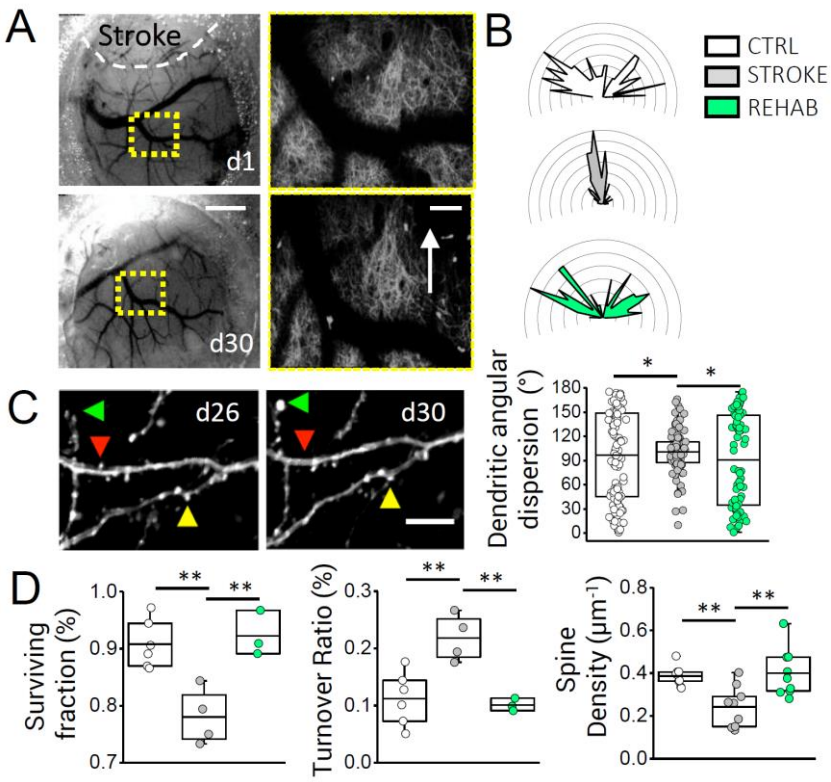

Figure 4: **Combined rehabilitation affects dendritic orientation and stabilizes spine turnover.** (A) Brightfield images showing the cranial window 1 day and 30 days after stroke (STROKE group). The rostral shift of cortical tissue due to the shrinkage of the stroke core is highlighted by the displacement of a reference point (i.e. blood vessel branching point) framed by the dotted yellow square. Scale bar = 1 mm. The panels on the right show the stitched two-photon images (4x4 Maximum Intensity Projections, MIPs of 130x130x50 µm^3) acquired within the region framed by the respective yellow squares in the left panels. The white arrow highlights the alignment of dendrites and axons towards the stroke core. Scale bar = 100 µm. (B) A polar plot showing the angular distribution of dendrites in the peri-infarct area. The plots are oriented as in Fig. 4A, where the lesioned area is toward the uppermost center of the plot. The box and whiskers plot below shows the higher angular dispersion of dendrites of the REHAB group compared to STROKE mice (for all panels, $Nmice_{CTRL}$ = 6, $Nmice_{STROKE}$ = 4, $Nmice_{REHAB}$ = 3; Dendritic angular dispersion: DAD_{CTRL}=97 ± 5, DAD_{STROKE}=101 ± 3, DAD_{REHAB}=91 ± 7; Homogeneity of variance test, Levene's test F=66.5). (C) MIPs of two-photon stacks (z depth 8 µm) of dendritic branches at 26 and 30 days after stroke (STROKE group). The arrows point to a newly formed (green), lost (red), and stable (yellow) spine. Scale bar = 5 µm. (D) Spine plasticity in the peri-infarct area. Box and whiskers plot showing the surviving fraction (SF) ± SEM (*left*; SF_{CTRL}= 0.93 ± 0.03%; SF_{STROKE}= 0.80 ± 0.04%; SF_{REHAB}= 0.92 ± 0.02%; one-way ANOVA with post hoc Bonferroni test, $P_{CTRL/STROKE}$ = 0.003, $P_{REAHB/STROKE}$ = 0.005), the turnover ratio (TOR) ± SEM (*middle*; TOR_{CTRL}= 0.11 ± 0.02%; TOR_{STROKE} = 0.20 ± 0.04%; TOR_{REHAB}= 0.10 ± 0.01%; one-way ANOVA with post hoc Bonferroni test, $P_{CTRL/STROKE}$ = 0.007, $P_{REAHB/STROKE}$ = 0.01) and spine density (SD) ± SEM (*right panel*; SD_{CTRL}= 0.39 ± 0.01 µm^{-1}; SD_{STROKE}= 0.24 ± 0.03 µm^{-1}; SD_{REHAB}= 0.40 ± 0.04 µm^{-1}; one-way ANOVA with post hoc Fisher test, $P_{CTRL/STROKE}$ = 0.006, $P_{REAHB/STROKE}$ = 0.003) in the peri-infarct area.

As ischemic damage-induced alterations in neural microcircuitry are known to affect dendrites as well as synaptic contacts, producing a large increase in spine turnover in the peri-infarct area[26, 27], we next asked wheatear rehabilitation might counteract the decreased stability of synaptic contacts. We thus monitored the appearance and disappearance of apical dendritic spines (Fig. 4C) by performing a frame-by-frame comparison of spines in the mosaic we acquired along the rostro-caudal axis with TPFM. Spines in the peri-infarct region of REHAB animals exhibited increased synaptic stability (Fig. 4D, left panel) and a lower turnover (Fig. 4D, middle panel) than STROKE mice, thereby recapturing features of pre-stroke conditions. The combined rehabilitative treatment also resulted in higher synaptic densities that were comparable to healthy CTRL values (Fig. 4D, right panel). The stabilization of synaptic contacts induced by the rehabilitation intervention was stronger at the proximal level and weakened with increasing distance from the ischemic core (Supplementary Fig. 5D, upper and middle panels). On the other hand, the change in density of spines extended beyond the peri-infarct region (Supplementary Fig. 5D, lower panel).

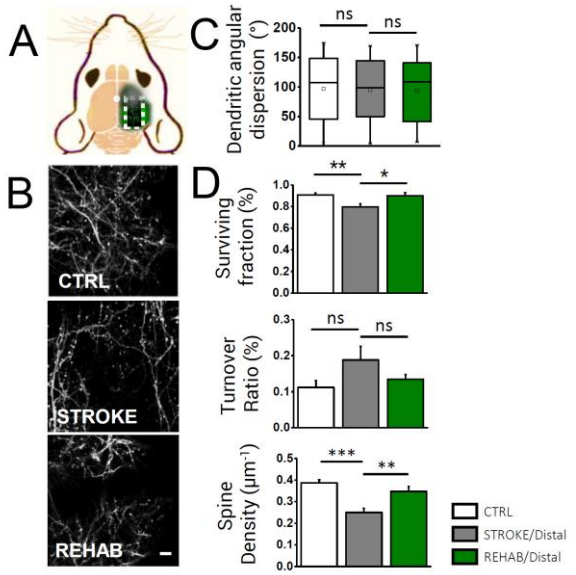

Supplementary Figure 5: **In vivo imaging of dendritic and spine plasticity in regions proximal and distal from stroke core**. (A) A schematic representation of the field of view (i.e. area within the white dotted square) of two-photon imaging of dendritic and spine plasticity in GFPM mice. The red spot indicates the site of the stroke lesion. (B) Representative examples of maximum intensity projection of two-photons stacks of dendritic branch orientation in the peri-infarct area in the CTRL, STROKE and REHAB groups. Scale bar = 10 µm. (C) A box plot showing the angular dispersion of dendrites in distal regions from the stroke core for both the STROKE and the REHAB animals. ($Nmice_{CTRL}$= 6, $Nmice_{STROKE}$ = 4, $Nmice_{REHAB}$= 3; Dendritic angular dispersion: DAD_{CTRL}=97 ± 5, $DAD_{STROKE\ Distal}$=95 ± 5, $DAD_{REHAB\ Distal}$=93 ± 6; Homogeneity of variance test, Levene's test, F=0.74; ns, not significant). (D) Histograms showing the SF (*upper panel;* $Nmice_{CTRL}$= 6, $Nmice_{STROKE}$ = 4, $Nmice_{REHAB}$= 3; SF_{CTRL}= 0.92 ± 0.02%; $SF_{STROKE\ Distal}$= 0.80 ± 0.03%; $SF_{REHAB\ Distal}$= 0.90 ± 0.03%; one way ANOVA with post hoc Bonferroni: ** *P* =0.007, * *P* =0.023), TOR (*lower panel;* $Nmice_{CTRL}$*= 6,* $Nmice_{STROKE}$ *= 4,* $Nmice_{REHAB}$*= 3;* TOR_{CTRL}= 0.11 ± 0.02%; $TOR_{STROKE\ Distal}$ = 0.19 ± 0.04%; TOR_{REHAB}= 0.13 ± 0.01% t-test: one way ANOVA with post hoc Bonferroni: not significant for all comparisons) and spine density (SD) (*right panel*; $Nmice_{CTRL}$= 3, $Nmice_{STROKE}$ = 3, $Nmice_{REHAB}$= 3; SD_{CTRL}= 0.39 ± 0.01 μm^{-1}; SD_{STROKE}= 0.25 ± 0.02 μm^{-1}; SD_{REHAB}= 0.35 ± 0.02 μm^{-1}; one-way ANOVA with post hoc Fisher test, $P_{CTRL/STROKE}$ = 0.0001, $P_{REHAB/STROKE}$ = 0.005) in the distal region (>1000 µm from the stroke core). Data are means ± SEM.

In brief, the longitudinal imaging of cortical neurons revealed that the combined rehabilitative therapy helped preserving the organization of dendritic arbors in peri-infarct cortex and restored dendritic spine plasticity to control levels.

Discussion

In the present study, we utilized optical imaging and techniques to manipulate neural activity to obtain a 'big picture' view of rehabilitation-induced cortical remodeling in the lesioned and healthy hemispheres of mice with photothrombotic stroke, and then explored synaptic characteristics of these cortical areas. We show that rehabilitative treatment combining physical training and pharmacological inhibition of the contralesional hemisphere stabilized perilesional synaptic contacts, while restoring features of cortical activation typical of pre-stroke conditions, and promoted the formation of an

enriched vascular environment to feed the neuronal population that have been newly recruited to motor functions in the peri-lesional area. To the best of our knowledge, our results provide the first evidence of the correlation between rehabilitation-induced neuronal and vascular reshaping in the mouse cortex after stroke.

The rehabilitation paradigm used in this study takes advantage of a combination of robotic rehabilitation and transient silencing of the healthy homotopic hemisphere with BoNT/E.

A recent study (Spalletti et al., under revision) tested how synaptic blockade in the healthy side by BoNT/E could induce improvements in motor functionality. The authors showed that BoNT/E silencing was active in the motor cortex for about 10 days after injection and produced a small and transient improvement in general forelimb motor tests (Gridwalk and Schallert Cylinder test). They hypothesize that silencing of the contralesional motor area stimulates plastic reorganization in perilesional tissue, but the enhancement of plasticity without the guide of an appropriate motor rehabilitation regime is not sufficient to achieve a complete recovery.

Robotic-assisted rehabilitation has received increasing attention in clinical practice in the last years since it allows repeatable and customizable motor training, while ensuring objective measures of motor performance[48-51]. Here we employed the M-Platform, a mechatronic device for mouse forelimb training[35] that mimics a robot for upper limb rehabilitation in humans, the "Arm-Guide"[52]. The same study from Spalletti and colleagues (under revision) demonstrated that this robotic rehabilitation paradigm per se was not able to generalize recovery to untrained motor tasks (i.e. Schallert Cylinder test). In our study, robotic rehabilitation alone was not sufficient to restore basic features of cortical activation like amplitude and promptness of the response. Given the uncomplete rescue produced by the single treatment demonstrated both at the behavioral and cortical level, in the following steps of the present study we focused on the combinatorial therapy that couples BoNT/E treatment with robotic training.

We first investigated the changes induced by the combined rehabilitation paradigm on cortical activity. It has been reported that motor-targeted focal stroke induces abnormally scattered or diffuse structures on cortical motor maps that persist for more than one month after stroke (see, for example, Harrison *et al*. 2013[21]). The diffuse structure of the motor maps we also observed in non-treated, post-acute stroke afflicted animals (STROKE group) is thought to represent the ongoing reorganization of the underlying cortical circuitry after stroke. In our combined rehabilitation paradigm, the re-establishment of a cluster of neuronal activity in peri-infarct areas reinstated location, timing and amplitude parameters that highly resembled those of healthy control animals. One limitation of the present study is the low spatial resolution of wide field calcium imaging, where the fluorescence recorded in each pixel is a convolution of dendritic and axonal activation signals from different cortical layers. The high resolution of TPFM might in the future show at the single cell level the origin of the new rehabilitation-induced functional patterns. This technique will allow, for example, determining if the increase in the amplitude of calcium signals we show in REHAB mice is due to a rise in the average activity of few excitatory neurons or if more cells are recruited in the peri-infarct area to control forelimb movements. The plastic reshaping of cortical motor representations that takes place in the subacute phase after stroke may be linked to the spared or newly sprouted cortico-spinal fibers[53, 54] or the myelination of transcallosal fibers[54]. Large scale imaging techniques like light sheet microscopy[55, 56] or diffusion magnetic resonance imaging[57] of axonal projections directed to and emerging from perilesional neurons will permit answering many questions related to the structural underpinning of functional rewiring.

By performing optogenetic stimulation on the same stroked-afflicted, rehabilitated mice, we demonstrated that the progressive spatial and temporal refocusing of motor control in the ipsilesional cortex is associated with increased interhemispheric coupling. The connectivity between homotopic motor cortices was restored 4 weeks after injury in STROKE mice, suggesting that some form of spontaneous recovery compensated for the transcallosal projections lost after stroke. The interhemispheric coupling is further enhanced after the rehabilitative therapy, suggesting a possible correlation between the recovery of the neuronal activation profiles in the perilesional area and the reinforcement of the connectivity with pyramidal neurons that project from the healthy M1. While there are no studies examining, on the same animals, cortical functionality and transcallosal connectivity to draw direct comparisons with, our results are consistent with the hypothesis that rehabilitative training of the paretic upper limb can, on one side, increase the functional activation of motor regions of the ipsilesional cortex[58, 59] and, on the other, decrease interhemispheric inhibition from the contralesional motor cortex[60]. We speculate that refocusing of the motor representation could be supported by dendritic rewiring in the peri-lesional area (as shown by our in vivo imaging result on structural plasticity), as well as by the activity of contralesional pyramidal cells projecting to the peri-infarct area. Further analysis on targeted neuronal populations is needed to clarify how rehabilitation-induced changes in transcallosal response are specifically linked to alterations in the excitatory/inhibitory balance in the ipsilesional spared tissue.

The mouse model of stroke used in this study provides several advantages over more traditional models. Previously, voltage-sensitive dyes has been combined with optogenetics to investigate cortical functional connectivity[31]. Recently, this approach applied to stroke models has demonstrated a spontaneous partial recovery of cortical functional connectivity 8 weeks after injury[30]. Our model, which combines transgenic GCaMP6 mice with AAV-induced expression of ChR2 in the homotopic M1, has the advantage of enabling, on one side, the reliable control and, on the other, the stable monitoring of neuronal activity over weeks and months. We anticipate that the all-optical approach we used will be further extended to the longitudinal exploration of the modified transcallosal axonal projections from the injured to the heathy hemisphere in our rehabilitation paradigm. Moreover, future investigations will help determine how the plasticity of subcortical regions (e.g. basal ganglia, thalamus) is involved in the modulation of rehabilitation-induced motor recovery. Cannula windows[61], fiber-optic systems[62, 63] or three photon imaging[64] will be optimal tools to image and manipulate neuronal activity in deep structures of the brain.

We hypothesized that the cortical motor circuit reshaping and refinement we observed in rehabilitated mice could be supported by angiogenesis and vascularization. This assumption is based on the relationship existing between the proangiogenic state and neurological improvement in patients with stroke[65-67]. The reason behind it could be that the region of active neovascularization acts as a niche for enhanced neuronal remodeling and tissue repair[68, 69]. Here, we measured an increase in vascular density after stroke localized in the peri-infarct area that is comparable to healthy animals in stroke non-treated mice (STROKE), while exceed physiological values in mice under double treatment (REHAB). Our results suggest that the transient proangiogenic state induced in response to an ischemic insult is enhanced by rehabilitation. In conjunction with the more efficient neuronal activation we measured in the same areas, our study thus supports the hypothesis that enduring recovery from stroke might result from the association of angiogenesis with neuronal plasticity[70]. We aim to extend the study on vasculature remapping by taking advantage of macro-scale imaging techniques like light-sheet microscopy. This technique, combined with appropriate clearing agents will allow investigating modification of the cytoarchitecture in the entire mouse brain with subcellular resolution[71-73] induced by rehabilitation after stroke.

A commonly agreed hypothesis is that the genesis of an enriched vascular milieu around the infarct area might promote synaptogenesis and dendritic remodeling, in addition to axonal sprouting[43, 74, 75]. In

parallel, a recent review by Wahl and colleagues suggested that rehabilitative training might shape the spared and the new circuits by selecting and stabilizing the active contacts and pruning the non-functional ones[14]. Alongside with these hypotheses, we show that increased vascular density is associates with increased the density of synaptic contacts and stabilization of synaptic turnover induced by the combined rehabilitative treatment. Although there are no other in vivo studies examining rehabilitation-induced spine plasticity after stroke to make a comparison with, our results are also in agreement with recent postmortem histological studies where rehabilitation was shown to determine significant increases in spine density of distal apical dendrites in corticospinal neurons[76].

Finally, our results show that the combined treatment preserves the random-oriented dendritic architecture at the end of the motor training period. One caveat that our study did not address is whether the random orientation of dendrites and axons was present from an earlier period after stroke, meaning that a shorter training might be sufficient to recover this structural feature. Alternatively, the pre-stroke organization could be recovered after a transient epoch of neurite alignment towards the stroke core. Further investigations will be necessary to resolve these questions.

In this study, we have shown for the first time that combined rehabilitation promotes the recovery of structural features and characteristics of healthy neuronal networks. The restorative therapy rescued the random orientation of pyramidal neurons and supported the stabilization of synaptic contacts. Indeed, rehabilitation counterbalanced the increased synaptic turnover induced by stroke by reinstating baseline dynamics.

Our multi-scale investigation brought to light complementary aspects of the structural and functional plasticity induced by rehabilitation that may lead to the development of more efficient therapies and improve post-stroke recovery in patient populations.

Online Methods

Mice

All procedures involving mice were performed in accordance with the rules of the Italian Minister of Health. Mice were housed in clear plastic cages under a 12 h light/dark cycle and were given *ad libitum* access to water and food. We used two different mouse lines from Jackson Laboratories (Bar Harbor, Maine USA): Tg(Thy1-EGFP)MJrs/J (referred to as GFPM mice) for two-photon imaging experiments and C57BL/6J-Tg(Thy1GCaMP6f)GP5.17Dkim/J (referred to as GCaMP6f mice) for wide-field and optogenetics. Both lines express a genetically-encoded fluorescent indicator controlled by the Thy1 promoter. A subset of GFPM mice imaged for the structural plasticity experiment (dendrites and spines analysis) were used for blood vessels evaluation; a subset of GCaMP6f mice previously used for calcium imaging were analyzed for inter-hemispheric connectivity. Each group contained comparable numbers of male and female mice, and the age of mice was consistent between the groups (4-12 months).

Photothrombotic stroke induction

All surgical procedures were performed under Zoletil (50 mg/kg) and xylazine (9 mg/kg) anesthesia, unless otherwise stated. After checking by toe pinching that a deep level of sedation had been reached, the animals were placed into a stereotaxic apparatus (Stoelting, Wheat Lane, Wood Dale, IL 60191). The skin over the skull was cut and the periosteum was removed with a blade. The primary motor cortex (M1) was identified (stereotaxic coordinates +1,75 lateral, -0.5 rostral from bregma). Five minutes after intraperitoneal injection of Rose Bengal (0.2 ml, 10 mg/ml solution in Phosphate Buffer Saline (PBS); Sigma Aldrich, St. Louis, Missouri, USA), white light from an LED lamp (CL 6000 LED, Carl Zeiss Microscopy, Oberkochen, Germany) was focused with a 20X objective (EC Plan Neofluar NA 0.5, Carl Zeiss Microscopy, Oberkochen, Germany) and used to illuminate the M1 for 15 min to induce unilateral

stroke in the right hemisphere. Afterwards, the skin over the skull was sutured and the animals were placed in recovery cages until full recovery. The CTRL animals are not subjected to photothrombosis.

Optical windows

For the experiments on GCaMP6f mice, we performed a thinned skull preparation on the right hemisphere between bregma and lambda to create an optical window. After applying the local anesthetic lidocaine 2% (20 mg/mL), the skin over the skull and periosteum was removed. The skull over most of the right hemisphere was thinned using a dental drill. A cover glass and an aluminum head-post were attached to the skull using transparent dental cement (Super Bond, C&S). We waited at least 4-5 days after the surgery for the mice to recover before the first imaging session.

For the experiments on GFPM mice, we created a square (3x5 mm^2) cranial window centered laterally on the right M1 (+1.75 mm from bregma) and extending rostro-caudally from 1 mm posterior to the bregma to lambda. The protocol we followed for cranial window preparation was slightly modified from Holtmaat et al., 2009[77] and Allegra Mascaro et al., 2014[78]. Briefly, we administered anesthetized mice a subcutaneous injection of dexamethasone (0.04 ml per 2 mg/ml). The animals were then placed into a stereotaxic apparatus; after applying the local anesthetic lidocaine 2% (20 mg/mL), the skin over the skull was removed. Using a dental drill (Silfradent, Forlì-Cesena Italia), the border of the area of interest was thinned and the central part of the bone was then gently removed. The exposed brain was covered with a circular cover glass; the optical window was sealed to the skull with a mixture of dental cement and acrylic glue. Finally, an aluminum head-post was attached onto the skull using dental cement (Super Bond, C&S, Sun medical Moriyama City, Shiga, Japan). The surgery was followed by the first imaging session under the two-photon microscope. If the cranial windows were opaque on the second imaging session, the windows were removed and cleaned, and imaging was performed immediately afterwards. After the last imaging session, all animals were perfused with 150 mL of Paraformaldehyde4% (PFA, Aldrich, St. Louis, Missouri, USA).

Intracortical injections

We used a dental drill to create a small craniotomy over M1, which was identified by stereotaxic coordinates. Botulinum Neurotoxin E (BoNT/E) injections were performed during the same surgical session in which the photothrombotic lesions were created. We injected 500 nl of BoNT/E (80 nM) divided in 2 separate injections of 250 nl at (i) +0.5 anteroposterior, +1.75 mediolateral and (ii) +0.4 anteroposterior, +1.75 mediolateral at 700 µm cortical depth. For virus injections, we delivered 1 µl of AAV9-CaMKII-ChR2-mCherry ($2.48*10^{13}$ GC/mL) 700-900 µm deep inside the cortex. The skin over the skull was then sutured; the animals were placed in a heated cage (temperature 38°) until they fully recovered.

Motor training protocol on the M-Platform

Mice were allowed to become accustomed to the apparatus before the first imaging session so that they became acquainted with the new environment. The animals were trained by means of the M-Platform, which is a robotic system that allows mice to perform a retraction movement of their left forelimb[35]. Briefly, the M-Platform is composed of a linear actuator, a 6-axis load cell, a precision linear slide with an adjustable friction system and a custom-designed handle that is fastened to the left wrist of the mouse. The handle is screwed onto the load cell, which permits a complete transfer of the forces applied by the animal to the sensor during the training session. Each training session was divided into "trials" that were repeated sequentially and consisted of 5 consecutive steps. First, the linear actuator moved the handle forward and extended the mouse left forelimb by 10 mm (full upper extremity extension). Next, the actuator quickly decoupled from the slide and a tone lasting 0.5 s informed the

mouse that it should initiate the task. If the animal was able to overcome the static friction (approximately 0.2 N), it voluntarily pulled the handle back by retracting its forelimb (i.e. forelimb flexion back to the starting position). Upon successful completion of the task, a second tone that lasted 1 sec was emitted and the animal was given access to a liquid reward, i.e. 10 µl of sweetened condensed milk, before starting a new cycle.

To detect the movement of the wrist of the animal in the low-light condition of the experiment, an infrared (IR) emitter was placed on the linear slide, and rigidly connected to the load cell and thus to the animal's wrist. Slide displacement was recorded by an IR camera (EXIS WEBCAM #17003, Trust) that was placed perpendicular to the antero-posterior axis of the movement. Position and speed signals were subsequently extracted from the video recordings and synchronized with the force signals recorded by the load cell (sampling frequency = 100 Hz).

All groups performed at least one week (5 sessions) of daily training, starting 26 days after injury for STROKE mice, 5 days after stroke for the ROBOT and REHAB group and after the surgery for CTRL animal.

Behavioral evaluation of forelimb use asymmetry

Spontaneous forelimb use was assessed in mice via the Schallert cylinder test. This test has been developed in rats and adapted for mice[37, 79]. Briefly, mice were placed individually inside a clean cylinder (diameter, 8 cm; height, 20 cm) that was placed vertically above a transparent surface and were allowed to explore this enclosure for 5 minutes. Mice were video- taped with a camcorder (C270, Logitech) that was positioned underneath the transparent surface. The number of paw touches on the wall during rearing was recorded offline, and the percentage use of each paw relative to the total amount of touches was calculated.

Optogenetic stimulation and simultaneous recording of GCaMP6f activity

After the last training session (i.e. 30 days after stroke and at least 2 weeks after the AAV injection in the CTRL group) mice were anesthetized under Zoletil (50 mg/kg) and xylazine (9 mg/kg) and placed into the stereotaxic holder. A small (2x2 mm^2) craniotomy was performed over the injected area. After placing the mouse under the wide field fluorescence microscope, we performed repeated laser (473 nm) stimulation (1-2 Hz, pulse duration 3-5 ms, pulse train duration 5 sec, laser power at the focal plane 5 mW) on the left M1, which was localized by mCherry fluorescence. Spurious activation of ChR2 from the green LED (used for GCaMP6f fluorescence excitation) was avoided by blocking half the illumination path with a shutter positioned after the collimator.

Wide-field fluorescence microscopy

The custom-made wide-field imaging setup was equipped with two excitation sources for the simultaneous imaging of GcaMP6f fluorescence and light-stimulation of ChR2. For imaging of GcaMP6f fluorescence, a 505 nm LED (M505L3 Thorlabs, New Jersey, United States) light was deflected by a dichroic filter (DC FF 495-DI02 Semrock, Rochester, New York USA) on the objective (2.5x EC Plan Neofluar, NA 0.085, Carl Zeiss Microscopy, Oberkochen, Germany). A 3D motorized platform (M-229 for xy plane, M-126 for z-axis movement; Physik Instrumente, Karlsruhe, Germany) allowed sample displacement. The fluorescence signal was selected by a band pass filter (525/50 Semrock, Rochester, New York USA) and collected on the sensor of a high-speed complementary metal-oxide semiconductor (CMOS) camera (Orca Flash 4.0 Hamamatsu Photonics, NJ, USA).

To perform optogenetic stimulation of ChR2, a 473 nm continuous wavelength (CW) laser (OBIS 473nm LX 75mW, Coherent, Santa Clara, California, United States) was overlaid on the imaging path using a second dichroic beam splitter (FF484-Fdi01-25x36, Semrock, Rochester, New York USA). The system

has a random-access scanning head with two orthogonally-mounted acousto-optical deflectors (DTSXY400, AA Opto-Electronic, Orsay France). A 20X objective (LD Plan Neofluar, 20x/0.4 M27, Carl Zeiss Microscopy, Oberkochen, Germany) was used to demagnify the image onto a 100X100 pxl^2 area of the sCMOS camera sensor (OrcaFLASH 4.0, Hamamatsu Photonics, NJ, USA). Images (512x512 pixels, pixel size 9 µm) were acquired at 25 Hz.

Two-photon fluorescence microscopy

The custom made apparatus for two-photon microscopy included a mode-locked Ti: Sapphire laser (Chameleon, Coherent Inc.) that supplied the excitation light. The laser beam was scanned in the xy-plane by a galvo system (VM500, GSI Lumonics). An objective lens (XLUM 20X, NA 0.95, WD 2 mm, Olympus) focused the beam onto the specimen. A closed-loop piezoelectric stage (PIFOC ND72Z2LAQ, PhysikInstrumente, Karlsruhe Germany) allowed axial displacements of the objective up to 2 mm with micrometric precision. Finally, the fluorescence signal was collected by a photomultiplier tube (H7710-13, Hamamatsu Photonics). Custom-made software was developed in LabVIEW 2013 (National Instruments).

.

Labelling of brain vasculature

The vasculature was stained using the protocol described by Tsai et al.[80], except that we replaced fluorescein (FITC)-conjugated albumin with 0.05% (w/v) tetramethylrhodamine (TRITC)-conjugated albumin (A23016, Thermo Fisher Scientific, Waltham, Massachusetts, USA) in order to avoid spectral overlap between GFP and FITC. Under deep anesthesia, mice were transcardially perfused first with 20-30 ml of 0.01 M PBS (pH 7.6) and then with 60 ml of 4% (w/v) paraformaldehyde (PFA) in PBS. This was followed by perfusion with 10 ml of fluorescent gel. After perfusion, a low temperature (ice cold) was maintained to ensure rapid solidification of the gel. After 30 min of cooling, the brain was carefully extracted to avoid damage to pial vessels, and it was incubated overnight in 4% PFA at 4 °C. Dissected cortices were cleared with thiodiethanol (166782 TDE, Sigma Aldrich, St. Louis, Missouri, USA)[81-83], specifically with serial incubation in 30% and 63% TDE/PBS for 1 h and 3 h, respectively, at room temperature. The cleared cortices were flattened using a quartz coverslip #No1 (UQG Optics).

Image analysis

Wide-field calcium imaging: during each experimental session, the mouse's head was restrained and placed on the M-platform under the wide-field microscope. To avoid head movement artefacts, each frame of the fluorescence stack was offline registered by using two reference points (corresponding to bregma and lambda) that were previously marked on the glass window during the surgery procedure.

For each stack (*FluoSt*) a median time series of GCamp6f fluorescence signal (*mF*) was extracted, where the value of mF at each *i-th* time point corresponded to the median value computed on all the pixels of the *i-th* frame of *FluoSt*. The *mF* was then oversampled and synchronized to the 100 Hz force and position signals.

The *mF* was used to define a GCamp6f fluorescence signal baseline F_0, which was identified by the concomitant absence of fluorescence and force signal deflections. F_0 was selected within a 2.5 ± 0.7 s interval (I) of 62 frames where the fluorescence signal was below 1 standard deviation (STD) of the whole *mF* signal and the corresponding force signal showed a value below of 1 STD of the whole recorded force signal. The fluorescence signal interval was used to reconstruct a 512x512 matrix, i.e. baseline matrix, in which the value of each pixel *B* of the *{m,n}* coordinates of the matrix was computed as follows:

$$B_{\{m,n\}} = median\left(p_{\{m,n\},j}\right) \;\; with\; j = 1, \dots, N_{\{I\}}$$

where $p_{\{m,n\},j}$ is the value of the pixel *p* of the *{m,n}* coordinates at the *j-th* frame of the interval I and $N_{\{I\}}$ is the length of Interval I. The baseline matrix was then used to normalize all the frames of the fluorescence stack *FluoSt*.

The noise-threshold of 1 STD of the whole recorded force signal was used as a measure of the force peaks exerted by the animal during the retraction task. According to Spalletti et al. 2013[84] , a force peak is defined as force values that transiently exceed the noise-threshold and result in a movement of the linear slide, as detected by variation of the position signal. To maintain consistency in this analysis, peaks of force that did not result in a movement of the slide were not considered.

The onset of each force peak was used as reference time point to select a sequence of 60 frames (2.4 s, where 0.4 s preceded the force peak) from the *FluoSt*. All sequences were visually checked to exclude possible spurious activation (e.g. early activation or no activation) from the analysis. All the selected sequences (*Seqs*) of the animal *An* on day *d* were compiled, defining a *stack of Seqs*, to compute the *Summed Intensity Projection* for the *An* at *d* ($SIP_{An\,d}$). The SIP is a matrix of 512x512 pixels, in which the value *P* of the pixel of the *{m, n}* coordinates is computed as follows:

$$P_{\{m,n\}} = \sum_{k=1}^{Ns} p_{\{m,n\},k}$$

where $p_{\{m,n\},k}$ is the value of the pixel p of the *{m, n}* coordinates at the *k-th* frame of *stack of Seqs,* and N_s is the number of frames of the *stack of Seqs*.

The most active area of the $SIP_{An\,d}$ was then detected by thresholding the $SIP_{An\,d}$ with a *median* ($SIP_{An\,d}$) + *STD* ($SIP_{An\,d}$) threshold value. The threshold $SIP_{An\,d}$ ($th\text{-}SIP_{An\,d}$) computed for each week of training on the M-Platform (d=1,…,4 of week W) was superimposed and the common areas, activated at least for 3 dailysessions out of 5 (60%), were labeled as "regions of interest" (ROIs) of the SIP_{An}. We further refined the analysis by dividing the image into two areas, and identifying one anterior ROI [-0.25 - +1.95 mm from bregma (B), AP] and one posterior ROI[+1.95 - + 4.15 mm from B, AP].

We also used the ROIs defined for each individual animal to identify the average ROIs among mice from the same experimental group: ROI_g with g = "CTRL", "STROKE", "ROBOT", "REHAB1w" and "REHAB4w" (see Supplementary Fig. 2B). Thus, the ROIs from animals of the same group were compiled and further thresholded (60%) to define the ROI_g. The extent of the ROI_g was computed as follows:

$$Area_{ROIg} = Area_p \text{ x } N_{ROIg}$$

where $Area_p$ corresponds to the area of a single pixel of the image (0.0086 mm^2) and N_{ROIg} is the number of pixels composing the ROI_g. Moreover, the centroid of each ROI_g was identified and its Euclidean distance from bregma was computed (Fig. 2F).

The ROIs defined for each individual animal were further used to extract the GCamp6f fluorescence signal corresponding to the activity of those areas. Indeed, from each frame of the *FluoS*, only pixels belonging to the selected ROI were considered when calculating the representative median value. Thus, a median time series, F_{ROI}, was extracted from the whole *FluoS* and was representative of the ROI. The fluorescence signal was normalized ($\frac{\Delta F_{ROI}}{F_0}\,100\% = \frac{\Delta F}{F}$) and low-pass filtered to clean the signal from the detected breathing artefacts (Chebyshev filter with cutting frequency = 9 Hz).

The previously detected force peaks were then used to select the GCamp6f fluorescence peaks from the $\frac{\Delta F_{ROI}}{F_0}$ signal. A time window that lasted 4 seconds, i.e. *wnd*, and was centered at the onset of the force peak, was used to delimit a part of the $\frac{\Delta F_{ROI}}{F_0}$ signal, i.e. F_{wnd}, to identify the corresponding fluorescence peak. A fluorescence peak was defined as the part of F_{wnd} that overcame the value of *median+3STD* calculated for the whole signal $\frac{\Delta F_{ROI}}{F_0}$. The onset of the peak was detected as

$$t_{\{peak\ onset\}} = t_{\left\{min\left(\frac{dF_{wnd}}{dt}\right)\right\}}$$

calculated for the $[t_{st}\ t_{max}]$ time interval, where t_{st} and t_{max} are the time points corresponding to the start of the *wnd* and the maximum of F_{wnd} , respectively.

From the fluorescence and force peaks, different parameters were computed as follows:

- the maximum of the peak (*Peak amplitude*).
- the *Slope* of the peak was defined as follows:

$$Slope_{\{peak\}} = max\left(\frac{dS}{dt}\right)$$

between the $t_{\{S\ peak\ onset\}}$and $t_{S\ max}$ where *S* = *fluo* or *force* signal.

- the time delay between the occurrence of the maximum of the fluorescence (*ΔT*).

The first movement time point was defined as the first variation of the position signal ($\left(\frac{dx}{dt}\right) > 0$) detected along the *wnd* interval.

Optogenetically-induced calcium activity: On every stack, we analyzed the calcium activity averaged over a round ROI (2.3 mm of diameter) centred on the peri-infarct area. Changing in the variation of fluorescence signal (ΔF/F) triggered by light irradiation of the contralateral hemisphere that were below 1% were excluded from the analysis. A calcium response was considered optogenetically-triggered if it started within 120 ms of optogenetic stimulation. The activation delay refers to the average (± Standard Error of the Mean, SEM) delay of the calcium peak with respect to the onset of laser stimulation. The success rate reports the number of times the laser stimulation successfully triggered contralateral activation over the total number of stimulation trials.

Two-photon imaging: For vessel orientation analysis, 1 mm deep stacks with 3 µm z-steps were acquired by Two Photon Fluorescence Microscope (TPFM). From these acquisitions throughout the entire cortical depth of the right hemisphere, we extracted maximum intensity projections (MIPs; 300 µm thick) over selected sub-stacks, avoiding meningeal vessels in the superficial 100 µm. Four MIPs of proximal regions (within 500 µm from the stroke core), and four MIPs of distal regions (1-1.5 mm from the core) for each mouse were analyzed. Polar plots of vessel orientation were obtained from the orientation analysis with the ImageJ plugin OrientationJ Distribution, using the Gaussian gradient with a Gaussian window of 3 pixels. Column plots were derived from manual analysis using the Angle tool in ImageJ (n = 30 vessels for each group). For the vessel density analysis, the stacks were first binarized using automatic thresholding with ImageJ. The sum of the pixel count from histograms of the binarized stacks was used as a measure of blood vessel density.

For the structural plasticity analysis of dendrites and spines of pyramidal neurons, we compared stacks in a vertical mosaic acquired in the rostro-caudal direction. During the last week of training (1st and 4th day), we acquired a mosaic of 100 µm thick stacks (113 x 113 μm^2) distanced 200 µm from each other along the rostro-caudal axis starting from the borders of the stroke core. We grouped stacks near (<500 µm) and far (from 1000 to 1500 µm) from the core, namely proximal and distal regions, respectively. Dendrite orientation was evaluated on 15 dendrites for each stack (on average) by measuring frame by frame the angle between each structure and the rostro-caudal axis. The stroke core was considered to be at 0°. For synaptic plasticity analysis, the fluorescence signal of a spine had to be be at least 1 standard deviation higher than the dendritic shaft fluorescence to be included in the analysis. We quantified the plasticity of dendritic spines using two functions: surviving fraction (SF) and turnover ratio (TOR)[77]; the SF describes the fraction of persistent structures:

$$SF(t) = N(t2) / N(t1)$$

where N(t1) is the number of spines present during the first imaging session (26 days after injury for STROKE and REHAB mice), while N(t2) indicates those structures that present 4 days after the first imaging session. The TOR evaluates the fraction of newly appeared in the images and disappeared structures:

$$TOR (t1, t2) = (Nnew + Ndisappear) / (N(t1) + N (t2))$$

where Nnew is the number of structures that are reported for the first time at time t2, Ndisappear is the number of structures that were present at time t1 but which are no longer present at time t2; N (t1) and N (t2) are the total of spines present on t1 and t2, respectively. Unless otherwise stated, data are reported as mean ± SEM.

Bibliography

1. Mozaffarian, D.*, et al.* Heart disease and stroke statistics--2015 update: a report from the American Heart Association. *Circulation* **131**, e29-322 (2015).
2. Carmichael, S.T., Kathirvelu, B., Schweppe, C.A. & Nie, E.H. Molecular, cellular and functional events in axonal sprouting after stroke. *Experimental neurology* **287**, 384-394 (2017).
3. Clarkson, A.N., Huang, B.S., Macisaac, S.E., Mody, I. & Carmichael, S.T. Reducing excessive GABA-mediated tonic inhibition promotes functional recovery after stroke. *Nature* **468**, 305-309 (2010).
4. Jones, T.A. & Adkins, D.L. Motor System Reorganization After Stroke: Stimulating and Training Toward Perfection. *Physiology* **30**, 358-370 (2015).
5. Bütefisch, C.M. Neurobiological bases of rehabilitation. *Neurological Sciences* **27**, s18-s23 (2006).
6. Di Pino, G.*, et al.* Modulation of brain plasticity in stroke: a novel model for neurorehabilitation. *Nature reviews. Neurology* **10**, 597-608 (2014).
7. Dancause, N. & Nudo, R.J. Shaping plasticity to enhance recovery after injury. *Progress in brain research* **192**, 273-295 (2011).
8. Plautz, E.J.*, et al.* Post-infarct cortical plasticity and behavioral recovery using concurrent cortical stimulation and rehabilitative training: a feasibility study in primates. *Neurological research* **25**, 801-810 (2003).
9. Adkins-Muir, D.L. & Jones, T.A. Cortical electrical stimulation combined with rehabilitative training: enhanced functional recovery and dendritic plasticity following focal cortical ischemia in rats. *Neurological research* **25**, 780-788 (2003).

10. Hesse, S.*, et al.* Combined transcranial direct current stimulation and robot-assisted arm training in subacute stroke patients: a pilot study. *Restorative neurology and neuroscience* **25**, 9-15 (2007).
11. Wang, R.Y.*, et al.* rTMS combined with task-oriented training to improve symmetry of interhemispheric corticomotor excitability and gait performance after stroke: a randomized trial. *Neurorehabil Neural Repair* **26**, 222-230 (2012).
12. Ward, N.S. & Cohen, L.G. Mechanisms underlying recovery of motor function after stroke. *Archives of neurology* **61**, 1844-1848 (2004).
13. Grefkes, C. & Fink, G.R. Reorganization of cerebral networks after stroke: new insights from neuroimaging with connectivity approaches. *Brain : a journal of neurology* **134**, 1264-1276 (2011).
14. Wahl, A.S.*, et al.* Neuronal repair. Asynchronous therapy restores motor control by rewiring of the rat corticospinal tract after stroke. *Science* **344**, 1250-1255 (2014).
15. Lee, J.K., Kim, J.E., Sivula, M. & Strittmatter, S.M. Nogo receptor antagonism promotes stroke recovery by enhancing axonal plasticity. *The Journal of neuroscience : the official journal of the Society for Neuroscience* **24**, 6209-6217 (2004).
16. Fang, P.C.*, et al.* Combination of NEP 1-40 treatment and motor training enhances behavioral recovery after a focal cortical infarct in rats. *Stroke* **41**, 544-549 (2010).
17. Soleman, S., Yip, P.K., Duricki, D.A. & Moon, L.D. Delayed treatment with chondroitinase ABC promotes sensorimotor recovery and plasticity after stroke in aged rats. *Brain : a journal of neurology* **135**, 1210-1223 (2012).
18. Gherardini, L., Gennaro, M. & Pizzorusso, T. Perilesional treatment with chondroitinase ABC and motor training promote functional recovery after stroke in rats. *Cerebral cortex* **25**, 202-212 (2015).
19. Caleo, M.*, et al.* Transient synaptic silencing of developing striate cortex has persistent effects on visual function and plasticity. *The Journal of neuroscience : the official journal of the Society for Neuroscience* **27**, 4530-4540 (2007).
20. Misgeld, T. & Kerschensteiner, M. In vivo imaging of the diseased nervous system. *Nat Rev Neurosci* **7**, 449-463 (2006).
21. Harrison, T.C., Silasi, G., Boyd, J.D. & Murphy, T.H. Displacement of sensory maps and disorganization of motor cortex after targeted stroke in mice. *Stroke* **44**, 2300-2306 (2013).
22. Winship, I.R. & Murphy, T.H. Remapping the somatosensory cortex after stroke: insight from imaging the synapse to network. *The Neuroscientist : a review journal bringing neurobiology, neurology and psychiatry* **15**, 507-524 (2009).
23. Brown, C.E., Aminoltejari, K., Erb, H., Winship, I.R. & Murphy, T.H. In vivo voltage-sensitive dye imaging in adult mice reveals that somatosensory maps lost to stroke are replaced over weeks by new structural and functional circuits with prolonged modes of activation within both the peri-infarct zone and distant sites. *The Journal of neuroscience : the official journal of the Society for Neuroscience* **29**, 1719-1734 (2009).
24. Sakadzic, S., Lee, J., Boas, D.A. & Ayata, C. High-resolution in vivo optical imaging of stroke injury and repair. *Brain research* **1623**, 174-192 (2015).
25. Sigler, A. & Murphy, T.H. In vivo 2-photon imaging of fine structure in the rodent brain: before, during, and after stroke. *Stroke* **41**, S117-123 (2010).
26. Brown, C.E., Li, P., Boyd, J.D., Delaney, K.R. & Murphy, T.H. Extensive turnover of dendritic spines and vascular remodeling in cortical tissues recovering from stroke. *The Journal of neuroscience : the official journal of the Society for Neuroscience* **27**, 4101-4109 (2007).
27. Mostany, R.*, et al.* Local hemodynamics dictate long-term dendritic plasticity in peri-infarct cortex. *The Journal of neuroscience : the official journal of the Society for Neuroscience* **30**, 14116-14126 (2010).
28. Brown, C.E., Li, P., Boyd, J.D., Delaney, K.R. & Murphy, T.H. Extensive Turnover of Dendritic Spines and Vascular Remodeling in Cortical Tissues Recovering from Stroke. *The Journal of Neuroscience* **27**, 4101-4109 (2007).

29. Johnston, D.G., Denizet, M., Mostany, R. & Portera-Cailliau, C. Chronic in vivo imaging shows no evidence of dendritic plasticity or functional remapping in the contralesional cortex after stroke. *Cerebral cortex* **23**, 751-762 (2013).
30. Lim, D.H., LeDue, J.M., Mohajerani, M.H. & Murphy, T.H. Optogenetic mapping after stroke reveals network-wide scaling of functional connections and heterogeneous recovery of the peri-infarct. *The Journal of neuroscience : the official journal of the Society for Neuroscience* **34**, 16455-16466 (2014).
31. Ayling, O.G., Harrison, T.C., Boyd, J.D., Goroshkov, A. & Murphy, T.H. Automated light-based mapping of motor cortex by photoactivation of channelrhodopsin-2 transgenic mice. *Nature methods* **6**, 219-224 (2009).
32. Cheng, M.Y., Wang, E.H. & Steinberg, G.K. Optogenetic approaches to study stroke recovery. *ACS chemical neuroscience* **5**, 1144-1145 (2014).
33. Tennant, K.A., Taylor, S.L., White, E.R. & Brown, C.E. Optogenetic rewiring of thalamocortical circuits to restore function in the stroke injured brain. *Nature Communications* **8** (2017).
34. Chen, T.-W.*, et al.* Ultrasensitive fluorescent proteins for imaging neuronal activity. *Nature* **499**, 295-300 (2013).
35. Spalletti, C.*, et al.* A robotic system for quantitative assessment and poststroke training of forelimb retraction in mice. *Neurorehabil Neural Repair* **28**, 188-196 (2014).
36. Krakauer, J.W., Carmichael, S.T., Corbett, D. & Wittenberg, G.F. Getting neurorehabilitation right: what can be learned from animal models? *Neurorehabil Neural Repair* **26**, 923-931 (2012).
37. Schallert, T., Fleming, S.M., Leasure, J.L., Tillerson, J.L. & Bland, S.T. CNS plasticity and assessment of forelimb sensorimotor outcome in unilateral rat models of stroke, cortical ablation, parkinsonism and spinal cord injury. *Neuropharmacology* **39**, 777-787 (2000).
38. van Meer, M.P.*, et al.* Recovery of sensorimotor function after experimental stroke correlates with restoration of resting-state interhemispheric functional connectivity. *The Journal of neuroscience : the official journal of the Society for Neuroscience* **30**, 3964-3972 (2010).
39. van Meer, M.P., van der Marel, K., Otte, W.M., Berkelbach van der Sprenkel, J.W. & Dijkhuizen, R.M. Correspondence between altered functional and structural connectivity in the contralesional sensorimotor cortex after unilateral stroke in rats: a combined resting-state functional MRI and manganese-enhanced MRI study. *Journal of cerebral blood flow and metabolism : official journal of the International Society of Cerebral Blood Flow and Metabolism* **30**, 1707-1711 (2010).
40. Bauer, A.Q.*, et al.* Optical imaging of disrupted functional connectivity following ischemic stroke in mice. *NeuroImage* **99**, 388-401 (2014).
41. Carter, A.R.*, et al.* Resting interhemispheric functional magnetic resonance imaging connectivity predicts performance after stroke. *Annals of neurology* **67**, 365-375 (2010).
42. Ankarcrona, M.*, et al.* Glutamate-induced neuronal death: a succession of necrosis or apoptosis depending on mitochondrial function. *Neuron* **15**, 961-973 (1995).
43. Brown, C.E., Boyd, J.D. & Murphy, T.H. Longitudinal in vivo imaging reveals balanced and branch-specific remodeling of mature cortical pyramidal dendritic arbors after stroke. *Journal of cerebral blood flow and metabolism : official journal of the International Society of Cerebral Blood Flow and Metabolism* **30**, 783-791 (2010).
44. Carmichael, S.T., Wei, L., Rovainen, C.M. & Woolsey, T.A. New patterns of intracortical projections after focal cortical stroke. *Neurobiology of disease* **8**, 910-922 (2001).
45. Hsu, J.E. & Jones, T.A. Contralesional neural plasticity and functional changes in the less-affected forelimb after large and small cortical infarcts in rats. *Experimental neurology* **201**, 479-494 (2006).
46. Ueno, Y.*, et al.* Axonal outgrowth and dendritic plasticity in the cortical peri-infarct area after experimental stroke. *Stroke* **43**, 2221-2228 (2012).
47. Dancause, N.*, et al.* Extensive cortical rewiring after brain injury. *The Journal of neuroscience : the official journal of the Society for Neuroscience* **25**, 10167-10179 (2005).

48. Veerbeek, J.M., Langbroek-Amersfoort, A.C., Wegen, E.E.H.v., Meskers, C.G.M. & Kwakkel, G. Effects of Robot-Assisted Therapy for the Upper Limb After Stroke. *Neurorehabilitation and Neural Repair* **31**, 107-121 (2017).
49. Lo, K., Stephenson, M. & Lockwood, C. Effectiveness of robotic assisted rehabilitation for mobility and functional ability in adult stroke patients: a systematic review protocol. *JBI Database of Systematic Reviews and Implementation Reports* **15**, 39-48 (2017).
50. Caleo, M. Rehabilitation and plasticity following stroke: Insights from rodent models. *Neuroscience* **311**, 180-194 (2015).
51. Balasubramanian, S., Klein, J. & Burdet, E. Robot-assisted rehabilitation of hand function. *Current opinion in neurology* **23**, 661-670 (2010).
52. Reinkensmeyer, D.J., Takahashi, C.D., Timoszyk, W.K., Reinkensmeyer, A.N. & Kahn, L.E. Design of robot assistance for arm movement therapy following stroke. *Advanced Robotics* **14**, 625-637 (2001).
53. Carter, A.R.*, et al.* Upstream dysfunction of somatomotor functional connectivity after corticospinal damage in stroke. *Neurorehabil Neural Repair* **26**, 7-19 (2012).
54. van Meer, M.P.*, et al.* Extent of bilateral neuronal network reorganization and functional recovery in relation to stroke severity. *The Journal of neuroscience : the official journal of the Society for Neuroscience* **32**, 4495-4507 (2012).
55. Keller, P.J. & Dodt, H.-U. Light sheet microscopy of living or cleared specimens. *Current Opinion in Neurobiology* **22**, 138-143 (2012).
56. Silvestri, L., Bria, A., Sacconi, L., Iannello, G. & Pavone, F. Confocal light sheet microscopy: micron-scale neuroanatomy of the entire mouse brain. *Optics express* **20**, 20582-20598 (2012).
57. Chang, E.H.*, et al.* The role of myelination in measures of white matter integrity: Combination of diffusion tensor imaging and two-photon microscopy of CLARITY intact brains. *NeuroImage* **147**, 253-261 (2017).
58. Hodics, T., Cohen, L.G. & Cramer, S.C. Functional imaging of intervention effects in stroke motor rehabilitation. *Archives of physical medicine and rehabilitation* **87**, S36-42 (2006).
59. Hubbard, I.J.*, et al.* A Randomized Controlled Trial of the Effect of Early Upper-Limb Training on Stroke Recovery and Brain Activation. *Neurorehabil Neural Repair* **29**, 703-713 (2015).
60. Harris-Love, M.L., Morton, S.M., Perez, M.A. & Cohen, L.G. Mechanisms of short-term training-induced reaching improvement in severely hemiparetic stroke patients: a TMS study. *Neurorehabil Neural Repair* **25**, 398-411 (2011).
61. Howe, M.W. & Dombeck, D.A. Rapid signalling in distinct dopaminergic axons during locomotion and reward. *Nature* **535**, 505-510 (2016).
62. Miyamoto, D. & Murayama, M. The fiber-optic imaging and manipulation of neural activity during animal behavior. *Neuroscience Research* **103**, 1-9 (2016).
63. Pisanello, F.*, et al.* Dynamic illumination of spatially restricted or large brain volumes via a single tapered optical fiber. *Nat Neurosci* **advance online publication** (2017).
64. Ouzounov, D.G.*, et al.* In vivo three-photon imaging of activity of GCaMP6-labeled neurons deep in intact mouse brain. *Nature methods* (2017).
65. Arkuszewski, M., Świat, M. & Opala, G. Perfusion computed tomography in prediction of functional outcome in patients with acute ischaemic stroke. *Nuclear Medicine Review* **12**, 89-94 (2009).
66. Hermann, D.M. & Chopp, M. Promoting brain remodelling and plasticity for stroke recovery: therapeutic promise and potential pitfalls of clinical translation. *The Lancet Neurology* **11**, 369-380 (2012).
67. Xiong, Y., Mahmood, A. & Chopp, M. Angiogenesis, neurogenesis and brain recovery of function following injury. *Curr Opin Invest Dr* **11**, 298-308 (2010).
68. Shen, Q.*, et al.* Adult SVZ stem cells lie in a vascular niche: a quantitative analysis of niche cell-cell interactions. *Cell stem cell* **3**, 289-300 (2008).

69. Prakash, R. & Carmichael, S.T. Blood-brain barrier breakdown and neovascularization processes after stroke and traumatic brain injury. *Current opinion in neurology* **28**, 556-564 (2015).
70. Ergul, A., Alhusban, A. & Fagan, S.C. Angiogenesis: A Harmonized Target for Recovery after Stroke. *Stroke* **43**, 2270-2274 (2012).
71. Silvestri, L., Mascaro, A.L.A., Costantini, I., Sacconi, L. & Pavone, F.S. Correlative two-photon and light sheet microscopy. *Methods* **66**, 268-272 (2014).
72. Silvestri, L., Mascaro, A.L.A., Costantini, I., Sacconi, L. & Pavone, F.S. Exploring the brain on multiple scales with correlative two-photon and light sheet microscopy. *Proc Spie* **8948** (2014).
73. Lugo-Hernandez, E.*, et al.* 3D visualization and quantification of microvessels in the whole ischemic mouse brain using solvent-based clearing and light sheet microscopy. *Journal of Cerebral Blood Flow & Metabolism* **0**, 0271678X17698970.
74. Kelley, M.S. & Steward, O. Injury-induced physiological events that may modulate gene expression in neurons and glia. *Reviews in the neurosciences* **8**, 147-177 (1997).
75. Carmichael, S.T. Cellular and molecular mechanisms of neural repair after stroke: making waves. *Annals of neurology* **59**, 735-742 (2006).
76. Wang, L., Conner, J.M., Nagahara, A.H. & Tuszynski, M.H. Rehabilitation drives enhancement of neuronal structure in functionally relevant neuronal subsets. *Proceedings of the National Academy of Sciences of the United States of America* **113**, 2750-2755 (2016).
77. Holtmaat, A.*, et al.* Long-term, high-resolution imaging in the mouse neocortex through a chronic cranial window. *Nature protocols* **4**, 1128-1144 (2009).
78. Allegra Mascaro, A.L., Sacconi, L. & Pavone, F.S. Laser nanosurgery of cerebellar axons in vivo. *Journal of visualized experiments : JoVE*, e51371 (2014).
79. Baskin, Y.K., Dietrich, W.D. & Green, E.J. Two effective behavioral tasks for evaluating sensorimotor dysfunction following traumatic brain injury in mice. *Journal of neuroscience methods* **129**, 87-93 (2003).
80. Tsai, P.S.*, et al.* Correlations of neuronal and microvascular densities in murine cortex revealed by direct counting and colocalization of nuclei and vessels. *The Journal of neuroscience : the official journal of the Society for Neuroscience* **29**, 14553-14570 (2009).
81. Costantini, I.*, et al.* A versatile clearing agent for multi-modal brain imaging. *Scientific reports* **5**, 9808 (2015).
82. Aoyagi, Y., Kawakami, R., Osanai, H., Hibi, T. & Nemoto, T. A rapid optical clearing protocol using 2,2'-thiodiethanol for microscopic observation of fixed mouse brain. *PloS one* **10**, e0116280 (2015).
83. Staudt, T., Lang, M.C., Medda, R., Engelhardt, J. & Hell, S.W. 2,2'-thiodiethanol: a new water soluble mounting medium for high resolution optical microscopy. *Microscopy research and technique* **70**, 1-9 (2007).
84. Spalletti, M.*, et al.* Efficacy of lacosamide on seizures and myoclonus in a patient with epilepsia partialis continua. *Epileptic disorders : international epilepsy journal with videotape* **15**, 193-196 (2013).